LUND UNIVERSITY

Master of Science Thesis
HT2021

Optimization of Margins and Plan Robustness for Proton Therapy of Hodgkin's Lymphoma

Filip Hörberger

Supervisors

Anneli Edvardsson, Marika Enmark, Ingrid Kristensen, Karin Andersson, Lund

Medical Radiation Physics, Lund
Faculty of Science
Lund University
www.msf.lu.se

Popularized summery in Swedish

Minskad stråldos med mindre marginaler i behandling av Hodgkins lymfom

Strålning inom vården används till allt ifrån bedöma benbrott till att behandla cancer. Cancerbehandling med högenergetiskt ljus är den allra vanligaste typen av strålbehandling och brukar benämnas konventionell strålbehandling. Däremot har terapi med protoner blivit allt vanligare runt om i världen. Vid konventionell strålbehandling går energistrålen in i kroppen, genom tumören och ut på andra sidan. Patienten erhåller därav en stråldos längs hela strålen, där bland annat "utgångsdosen" kan påverka frisk vävnad bortom tumören. Eftersom protoner är tunga, laddade, partiklar frigör de sin energi på ett annat sätt i jämförelse med ljus och därmed blir också strålnings-utbredningen annorlunda. Protoner med en given energi färdas en väldefinierad sträcka innan de fullt bromsas in, där en stor del av energin frigörs mot slutet av sträckan. Detta kan användas i behandling sådan att den stora delen av energin sammanfaller med själva tumören. Efter att ha levererat stråldos till tumören bromsar protonerna in och ger därmed inte ett stråldosbidrag till frisk vävnad långt bakom tumören. På detta vis erhåller frisk vävnad i vissa fall en mindre stråldos och protonterapi kan vara ett bra behandlingsalternativ för tumörtillväxt nära känsliga områden som hjärnan, ögonen, hjärtat och ryggmärgen. En stor andel av de patienter som behandlas med protonterapi är därför barn och unga, eftersom det är för dessa risken med strålningsinducerade sena bieffekter är som högst.

Vid strålbehandling utgör cancercellerna en målvolym, vilken man vill ska erhålla en tillräckligt hög stråldos så att alla cancercellerna dör. Denna volym ska inkludera alla cancerceller, även de sub-kliniska cellerna som gömmer sig runt den cancertillväxt som går att urskilja med medicinska undersökningar. För att inkludera dessa expanderar man målvolymen med lite extra marginal i strålbehandlingsplanen. Vidare, på grund av organrörelse som till exempel andning, hjärtslag och tarmrörelse, ligger oftast målvolymen inte helt stilla. Detta innebär att ytterligare marginaler måste tilläggas runt målvolymen för att inkludera områden där tumören kan förflyttat sig till. Samtidigt som målvolymen förstoras är det viktigt att minimera stråldosen till normalvävnad samt till riskorgan. I och med detta uppstår alltså en konflikt eftersom större marginaler innebär högre sannolikhet att alla cancerceller dör men medför högre stråldos till normalvävnad och riskorgan. Vidare består en behandling oftast av flera fraktioner, där en del av behandlingen ges vid varje fraktion. Det är därför viktigt att samma behandlingssituation återskapas vid varje fraktion, inkluderat samma patientpositionering och vid behandling av Hodgkins lymfom även snarlika andetag vid varje fraktion. Snarlika andetag innebär att variationer av lungvolymen mellan flera andetag ska vara ganska liten vid behandling av Hodgkins lymfom.

I det här arbetet undersöktes det om mindre marginaler runt målvolymen kan användas samtidigt som målvolymen erhåller tillräckligt hög stråldos genom behandlingen. Arbetet gjordes med fokus på behandling för Hodgkins lymfom med protonterapi. Resultatet visade att mindre marginaler runt målvolymen är fullt rimligt för de patienter där endast en liten grad anatomiska skillnader förekom under behandlingen. För patienter med stora anatomiska skillnader ökade risken för att under-dosera målvolymen. Mindre stråldos till riskorgan är en värdefull vinst, men implementeras mindre marginaler kliniskt skulle justering av behandlingsplanen för patienter med stora anatomiska skillnader eventuellt behövas användas i mer utsträckning än vad som görs idag för att inte riskera under-dosera målvolymen.

Abstract

Purpose/Background: Utilizing proton therapy (PT) for treatment of Hodgkin's lymphoma (HL) has demonstrated favorable features, particularly a reduced dose to organs at risk (OAR) in comparison with photon radiotherapy. However, there is a coherent complexity with PT including its uncertainties, such as range-uncertainties and set-up variations as protons are highly sensitive to tissue density variations within the beam-path. These are mitigated by using beam-specific target-margins, robust-optimization (RO) and motion mitigation techniques such as Deep Inspiration Breath-Hold (DIBH). Currently, a symmetric 7 mm displacement and 4.5% range-uncertainty (7 mm/4.5%) is applied in the RO-process for HL patients. The purpose of this thesis was to evaluate if the margins for HL PT in DIBH could be reduced and still ensure a robust dose to the target volume, simultaneously as the dose to normal tissue and OARs was minimized.

Material and Methods: An evaluation of the original treatment plans (TP) and of TPs with smaller margins, based on a retrospective evaluation of weekly verification CTs (vCT) acquired throughout the treatment course, were conducted in this study. Nine patients, diagnosed with HL who received PT treatment with DIBH, were included. A geometric and dosimetric analysis of the original TPs, including the total lung volume variation as well as OAR doses and target coverage(CTV $D_{98\%}$), were performed by recalculating the original TPs on each acquired vCT to determine any deviations from the planning CT (pCT). Thereafter, three new TPs with smaller margins (5 mm/4.5%, 3 mm/4.5%, 5 mm/3.5%) were optimized and evaluated similar to the original TPs, i.e. with respect to target coverage and OAR doses.

Results: From the evaluation of the original TPs, both dosimetric and geometric variations throughout treatment were observed, with clinical target volume (CTV) $D_{98\%}$ deviations within 1-3 % for most patients as well as an increase and decrease in OAR doses of up to 5 and 1 Gy (RBE) respectively. In addition, relative lung volume deviations of up to 25% were observed. However, for one patient, CTV $D_{98\%}$ was as low as 86% with the original TP. For five out of the nine patients, TPs with smaller margins (5 mm/4.5%) would deliver a robust dose to CTV, with CTV $D_{98\%} \geq 96\%$. Two patients only scarcely achieved a robust dose to CTV throughout treatment with smaller margins. The last two patients already had insufficient target coverage with their original TP, which became more critical when applying smaller margins, e.g. CTV $D_{98\%}$ dropped from 86% to 70%. With smaller margins OAR doses were lowered by 0.1 - 1 Gy(RBE).

Conclusion: TPs with smaller margins, in particular TP 5 mm/4.5%, demonstrated a sufficient robustness to CTV and lower dose to OARs. On the other hand, smaller margins increase the risk for under-dosing CTV if the patients DIBH reproducibility is poor. Ideally, if implementing smaller margins, knowledge about the DIBH reproducibility at an early stage is required, and replanning would be required to a greater extent.

Acknowledgement

Special thanks goes to all that have helped me complete my master thesis and supported me, as well as to all the people on the radiation therapy department and those at my office at Skåne University Hospital for making me feel welcomed during my brief time at the department. However, I would like to express an extra gratitude towards my supervisors:

Annelie Edvardsson, thank you for all the ideas, encouragement and guidance along the way as well as your outstanding enthusiasm for RT. You have made this project such an interesting one, giving me the opportunity to learn a lot about RT.

Marika Enmark, thank you for your valuable inputs, enthusiasm and engagement in this study. You as well have made this project educational and fun to work on.

Ingrid Kristensen, thank you for your expertise and for answering all my questions regarding dose-planning. It has been very educational to discuss all dose-planning related questions with you.

Karin Andersson, thank you for all your valuable inputs, ideas, and contributions in all parts of this study. Especially for the contributions with the help in the evaluation of the image registration, an important first step in this project.

Abbreviations

3D-CRT - 3-Dimensional Conformal Radiation Therapy
AP - Anterior to Posterior
BSPTV - Beam-Specific Planning Target Volume
CT - Computer Tomography
CTV - Clinical Target Volume
DIBH - Deep Inspiration Breath Hold
DIR - Deformable Image Registration
DSC - Dice Similarity Coefficient
DVF - Deformation Vector Field
FB - Free Breathing
HD - Hausdorff Distance
HL - Hodgkin's lymphoma
HU - Hounsfield Units
IBA - Ion Beam Applications
IMRT - Intensity Modulated Radiation Therapy
ITV - Internal Target Volume
IR - Image Registration
LR - Left to Right
MFO - Multi-field Optimization
MU - Monitor Unit
NTCP - Normal Tissue Complications Probability
NUPO - Nonlinear Universal Proton Optimizer
OAR - Organ At Risk
PBS - Pencil Beam Scanning
pCT - planning Computer Tomography
PCS - Proton Convolution Superposition
PT - Proton Therapy
PTV - Planning Target Volume
RT - Radiotherapy
RIR - Rigid Image Registration
SI - Superior to Inferior
SOBP - Spread Out Bragg Peak
SFUD - Single Field Uniform Dose
TCP - Tumor Control Probability
TP - Treatment Plan
RBE - Relative Biological Effectiveness
RO - Robust Optimization
vCT - verification Computer Tomography

Contents

1 Introduction

Hodgkin's lymphoma (HL) is a malignant disease originating from the lymphatic system accounting for roughly 10% of all lymphatic diseases, with most patients being young adults (15–34 years)[1]. A second, smaller peak is also observed for older patients (>50 years). Typical symptoms are: enlarged and sore lymph nodes, weight-loss, night sweats and fever. Additionally, as tumor growth is often located in the thorax region, in the mediastinal area, patients often experience shortness of breath and pressure in the chest area. With new developments in the last couple of decades in treatment of HL, the prognosis for most patients have turned from incurable into a favorable prognosis with survival rates above 80-90% [2]. This success is mostly due to the introduction of combined modality treatment where patients first undergo intensive chemotherapy followed by radiotherapy (RT). However, both chemotherapy and RT have demonstrated long-term side effects. For example, late toxic effects of RT for treatment of HL consists of secondary cancer, lung disease and cardiovascular disease[3]. As most patients are young adults with favorable survival rates, these late effects are of great concern and finding ways to reduce treatment associated side-effects have therefore been the major goal of modern research in treatment of HL.

In consideration of long term side effects, the focus of modern HL treatment has been achieving a high tumor control while simultaneously reducing the risk of long term effects, realized through a reduction of the irradiated volume and the prescribed dose[3][4]. With treatment techniques such as 3-dimensional conformal radiation therapy (3D-CRT) and intensity modulated radiation therapy (IMRT), which utilize multiple photon fields, further improvements were made and a more conformal dose distribution could be generated, sparing the dose to organs at risk (OAR) even further. However, this came at the expense of irradiating a larger volume, often consisting of normal tissue, with low doses (termed low-dose bath). Other dose delivery techniques where the low-dose bath can be minimized without compromising coverage or conformality over the target volume is therefore desirable. Utilizing protons, with their well-defined range and precipitous dose-drop beyond that range, i.e. proton therapy (PT), presents another treatment option to generate a conformal dose distribution and further OAR sparing in comparison to photon therapy[4][5]. Due to these properties, PT can under the right conditions have a positive impact in the treatment of mediastinal HL.

For most HL patients delivering PT in Deep Inspiration Breath Hold (DIBH) can further reduce dose to OARs and other normal tissue since the target volume is placed further away from OARs throughout irradiation[4][5]. However, it is important to understand the increased complexity of PT including its uncertainties, such as patient positioning and proton range[5][6]. In practice, these uncertainties are mitigated with treatment volume-margins and robust-optimization (RO) to ensure a robust dose. As every diagnosis, including HL, provides its own unique target location, treatment margins are individually determined with respect to the location. For HL patients treated at the Swedish proton center, the Skandion clinic (Uppsala, Sweden) through Skåne University Hospital, a target volume margin of 7 mm and proton range-uncertainty of 4.5% is used[7]. However, it is of interest to evaluate if these margins can be further optimized in order to ensure a robust dose to the target volume, simultaneously as the dose to normal tissue and OARs is minimized.

1.1 Purpose

The purpose of this thesis was to optimize treatment margins for HL PT treatment delivered in DIBH such that a robust dose is delivered to the target volume while simultaneously minimizing the dose received by normal tissue and OARs. This was based on a retrospective evaluation of weekly verification CTs acquired throughout the treatment. Good target coverage is in direct conflict with dose to OARs and by further optimizing treatment-margins used clinically today these doses can potentially be minimized. This is important as most patients diagnosed with HL are young adults and reducing treatment associated side-effects is the major goal of modern research for treatment of HL.

2 Background

2.1 Proton Radiotherapy

The aim of any radiation treatment is achieving high tumor control probability (TCP), i.e. destroying the tumor, while minimizing the normal tissue complications probability (NTCP), i.e. sparing OARs and normal tissue, as much as possible[8]. In conventional RT with photons, normal tissue in close proximity to the target volume will receive a substantial amount of dose due to the physical properties of photons. With photons, the dose as a function of depth will initially increase up to a maximum and thereafter decline exponentially, consequently, a photon beam will deposit a dose all the way from entering to exiting the patient's body. This property arises because the individual photon can traverse a long distance before it interacts with matter. Protons on the other hand, being a heavy charged particle, continuously lose their energy as a function of depth[9]. The rate at which energy is deposited per unit distance (defined as Linear Energy Transfer) increases as the velocity of the protons decreases, being inversely proportional to the square of the protons velocity. Henceforth, protons with a given energy will lose their energy at a growing rate as they are slowing down, increasing rapidly at the end of their track. Protons with a given initial energy will therefore traverse a well-defined range before coming to an abrupt stop. Additionally, at this range a narrow region will be formed where the dose deposition peaks followed by a precipitous dose-drop, with a negligible dose deposit beyond that range, dropping to zero within a few millimeters[10]. This characteristic depth-dose curve is referred to as a "Bragg curve" with the peak of dose deposition defined as the Bragg peak.

PT with only monoenergetic protons, i.e. a single Bragg peak, would not be suitable for RT due to insufficient coverage of the target volume[11]. However, an accumulation of dose depositions from protons with various energy and intensity can be used to produce a Spread-Out Bragg peak (SOBP), since protons with higher energies generate Bragg peaks at a greater depth. The SOBP is generated such that sufficient coverage of the target volume is obtained. The difference in depth-dose between photons and protons is illustrated in figure 1, as well as an example of an SOBP.

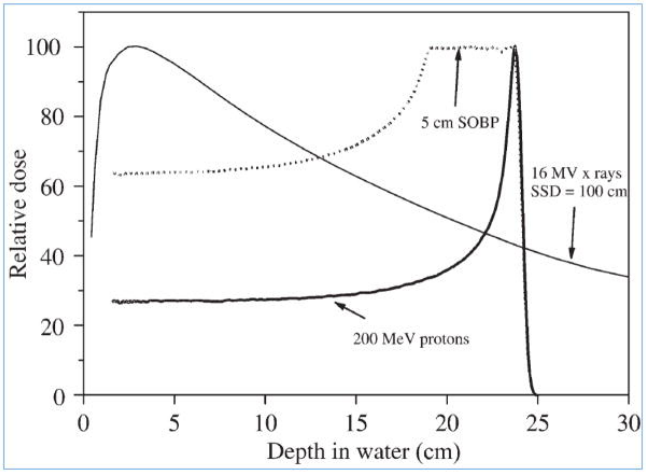

Figure 1: Comparison of depth dose curves between a 200 MeV proton beam, a 16 MV X-ray beam, as well as a 5 cm Spread-Out Bragg Peak. Each curve is normalized such that the maximum dose is located at 100% [9].

By utilizing the lower entrance dose, intense dose peak and precipitous dose-drop beyond that peak from protons in RT, a reduced total integral dose imparted to surrounding normal tissue in comparison to photons is obtained[10]. Additionally, normal tissue and OARs behind the SOBP can be spared from receiving dose. In comparison with older PT techniques (Passive scattering proton therapy) and conventional RT, this effect is even more pronounced with Pencil Beam Scanning (PBS) systems where particularly high dose gradients can be achieved. PBS consists of a sharp pencil beam with a finite beam size and by using magnetic fields the PBS proton beam is swept laterally and orthogonal relative the beam direction, generating a layer[9]. Using various energies, dose is deposited layer by layer through a step and shoot technique, where within each layer individual spots are delivered one spot at the time. Consequently, a 3D dose distribution will be generated as the superposition of all the pencil beams. In figure 2 the difference in dose distribution of PT and a photon RT treatment plan for a HL target is displayed. Additionally, the photon treatment plan is a 3DCRT meaning that a higher dose-conformality could be achieved with a IMRT but at the cost of the previously mentioned "low-dose bath" (see section 1).

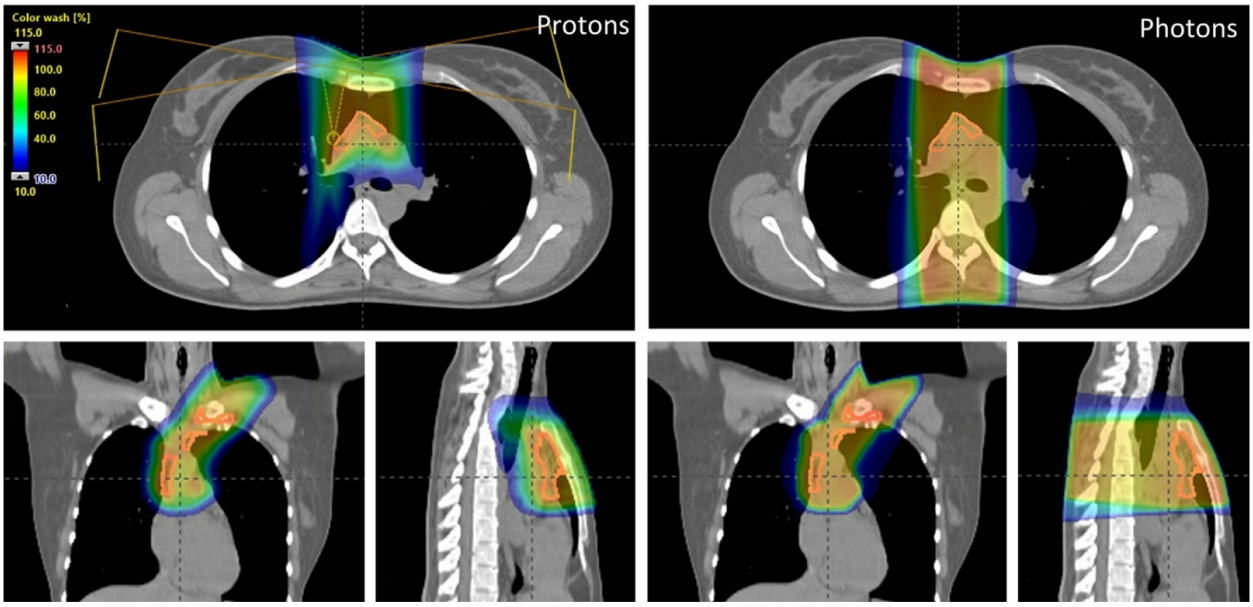

Figure 2: Difference in dose distribution between PT (left), delivered with PBS, and photon RT (right), delivered with 3DCRT, for HL treatment in the thorax region. The target volume is highlighted in pink whereas the dose-level in percent is located in the top left corner[12].

2.1.1 Uncertainties in Proton Therapy

The superior dose distribution of PT also has its dose delivery hazards as it is of great importance that the SOBP is delivered precisely at the desired target volume. Uncertainties such as increased sensitivity to range, changes in geometry and anatomy, interplay effects between dose-delivery and respiratory motion, beam path through heterogeneous tissues, makes this feat a challenging and complex problem[6]. The rate which protons lose their energy at a given position in the patient is estimated by converting the Hounsfield units (HU) of CT images into stopping powers. This introduces a range uncertainty with the potential of altering the proton range and the position of the Bragg peak, consequently, altering the dose distribution. Target volumes could potentially receive a lower dose or critical structures a higher one. Additionally,

geometrical uncertainties from setup errors or intra-fractional organ motion can cause displacements, moving a tumor(healthy tissue) partially/completely outside(inside) the Bragg peak. In contrast to photons where displacements only move the dose distribution, the resulting effect for protons could be a severely degraded dose distribution. Geometric displacement can also change tissue density along a given beam path, altering the range of protons traversing that path[6]. This is of great concern for treatment in the thorax region due to the magnitude of tissue density heterogeneity between the low-density lung tissue and surrounding water-equivalent tissue, as the density of solid tissue is about three times that of the lung parenchyma. Consequently, with the influence of respiratory motion, PT in the thorax region impose a major challenge. Henceforth, at the Skandion Clinic, PT in free breathing (FB) is excluded if target movement exceeds 5 mm[3].

2.1.2 Motion mitigation with Deep Inspiration Breath Hold

Uncertainties due to respiratory motion can be mitigated through beam gating techniques, e.g. DIBH, which if applied successfully have the potential to generate a geometrical situation that is almost static[13]. DIBH works by instructing the patient to take a deep breath such that they reach a certain amplitude and then hold their breath for 20-30 seconds. The dose is only delivered when they reach this amplitude, i.e. beam-gating, and by holding their breath respiratory motion is mitigated. For treatment in the mediastinal area the irradiation to heart and lung tissue is usually reduced when treatment is performed with DIBH[2][4]. However, it is not given that treatment with DIBH always leads to a more favorable dose distribution to all OARs and individualized evaluation is crucial. Furthermore, patients will need to undergo a number of breath-holds during each treatment fraction and small anatomical changes such as heart movement could potentially affect the reproducibility of these breath-holds, questioning the possibility to generate the same geometrical situation every breath-hold. In a study by Enmark et al[14], the variability of DIBH during PBS proton delivery was investigated. It was observed that the impact of inter-breath hold variations were minimal when averaged over a full series of fractions, an indication that DIBH is a suitable motion mitigation technique for PT in the thorax region. For treatment with DIBH at the Skandion clinic, the breath hold reproducibility is evaluated over a series of DIBH-CT images, one DIBH CT used for dose planning and two additional DIBH-CT scans. Images are evaluated in aspect of[15]:

- Baseline and breath-hold amplitude,
- Target position,
- Variation of lung volume,
- The position of the diaphragm and heart,
- Variation in body contour,

where baseline is the chest amplitude at which the patient returns to after every breath-hold. In order to mitigate other uncertainties, such as set-up and range uncertainties, margins and RO can be utilized which is further discussed in section 2.3.

2.1.3 Relative Biological Effectiveness

Radiation of various quality deposits their energy differently, consequently, the degree of biological effect will not be the same for equal absorbed doses when delivered with different radiations[16]. Radiation quality describes the type of particle/photon and their energy spectrum. For example, 1 Gy of proton radiation does not have the same biological effect as 1 Gy of photon radiation. Thus, it has become customary in radiation biology to define the Relative Biological Effectiveness (RBE) in order to quantify the difference in biological effectiveness between radiation qualities. RBE is defined as the ratio between two absorbed doses from different radiation qualities, given under identical conditions, resulting in the same biological effect, expressed as[16]:

$$RBE = \frac{D_{ref}}{D_x} \quad . \tag{1}$$

As the RBE concept should be unambiguous, the radiation quality of interest, D_x, is often compared with a "reference" radiation quality, D_{ref}, where ^{60}Co γ rays is predominately chosen as the reference radiation[16]. In theory, any absorbed dose delivered to a given RBE dose will produce the same biological effectiveness regardless of which radiation quality used. However, the RBE concept is an experimentally determined quantity which depends on chosen biological endpoint (e.g. cell survival or chromosome aberration) but also varies between different cell- and tissue-types[17]. Consequently, in PT an RBE value of 1.1 is recommended[18], which is an average RBE from several therapeutic proton energies and of a limited number of tissues. As such the same biological effectiveness is achieved with 10 Gy of protons as with 11 Gy of ^{60}Co γ rays.

2.2 Planning and verification CTs

External RT treatment starts with the acquisition of a planning medical image, e.g. a CT image. This image includes information about the patient's anatomy which a physician utilize to delineate target volumes and OARs. A treatment plan (TP) is thereafter optimized with the planning CT (pCT) image and the delineated volumes to achieve sufficient target coverage and adequate OAR sparing. However, external RT often consists of a multi-fractional treatment which can take up to several weeks and the conformal dose distribution achieved on the pCT-image represents only a snapshot of the patient's anatomy acquired some period before therapy start. This might not be a *true* representation of the patient's anatomy throughout treatment. Inter-factional variations, due to anatomical changes such as inflammations, disease progression/regression, physiological organ shape variation and/or weight changes, during the treatment course might degenerate the resulting, high, dose conformality previously achieved on the pCT[19]. Hence, verification CTs (vCT) are acquired before and during treatment and delineated contours are transferred with image registration (see section 2.6). The original dose-plan is then recalculated on the vCTs, where it is verified that the treatment criteria, such as CTV coverage and adequate OAR sparing, is still achieved. This is important as the vCTs represents the *present* anatomy of the patient. vCTs acquisition throughout treatment is an useful tool in any RT as inter-fractional changes and their effect on the resulting dose-distribution can be evaluated. If large deviation in the resulting dose-distribution is observed, replanning might be necessary. With replanning a new TP is optimized to better conform to the anatomical variations observed at the vCTs. A schematic illustration of treatment incorporating vCTs and replanning within the treatment is displayed in figure 3.

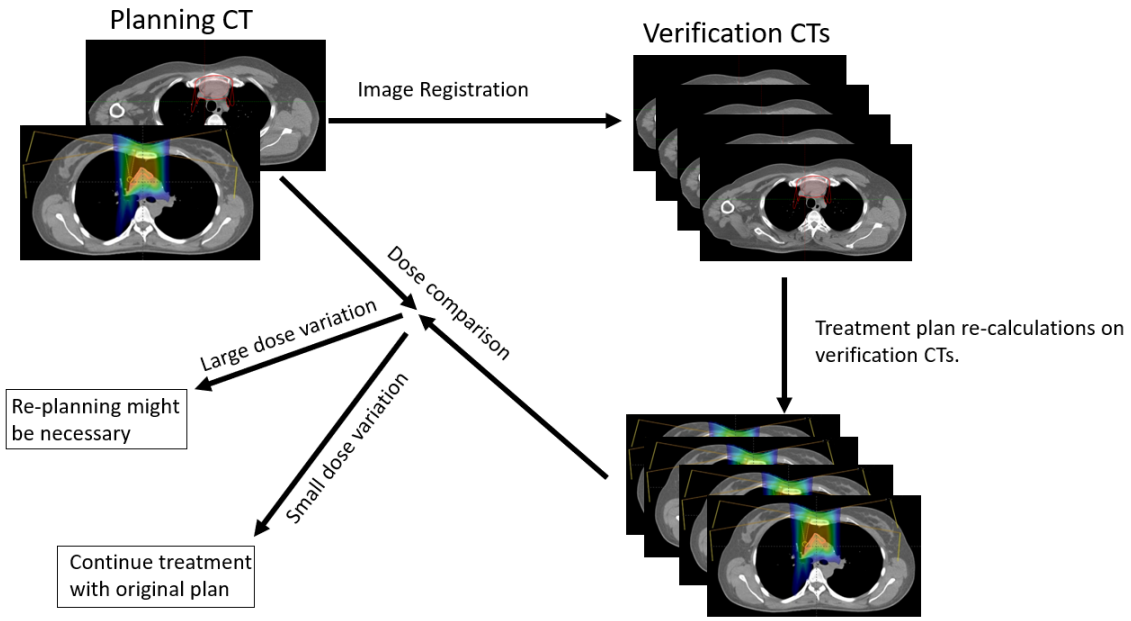

Figure 3: Schematic illustration of RT treatment flow, where the treatment plan is re-calculated on verification CTs to evaluate target coverage and adequate OAR sparing.

2.3 Target volumes and critical structures

A prerequisite for any meaningful 3D RT planning is defining volumes of interest. In order to avoid any ambiguity the International Commission on Radiation Units & Measurements (ICRU) has introduced several different target volumes and critical structures. According to ICRU Report No.50 and No.62[20][21] the volume at which a demonstrable malignant growth is seen from various imaging modalities is defined as the Gross Tumor Volume (GTV). To account for sub-clinical microscopic tumor growth around the clinical visible growth, a margin is added around the GTV. This enlarged volume is defined as Clinical Target Volume (CTV) and must be treated adequately as GTV to ensure the purpose of the treatment. However, the location of CTV can vary because of the motion from another organ(s) (lungs, bladder, intestinal system, etc.) and further margins are added to include this possible variation of CTV. Organ motion is thus incorporated within the extra margins placed around CTV and is referred to as the Internal Target Volume (ITV). In conventional RT with photons, a Planning Target Volume (PTV) is then created by assigning an additional safety margin to the CTV/ITV in order to ensure adequate dose coverage, accounting for geometrical variations during the course of treatment, e.g. set-up. Finally, it is also necessary to define OARs, those organs that are extra sensitive against radiation, for example medulla, which can significantly affect the choice of treatment and prescribed dose. A schematic illustration of these volume definitions, including OAR, are presented in figure 4. Treatment optimization is thereafter performed with respect to PTV and OARs, such that the PTV receives the prescribed dose while simultaneously sparing the OARs.

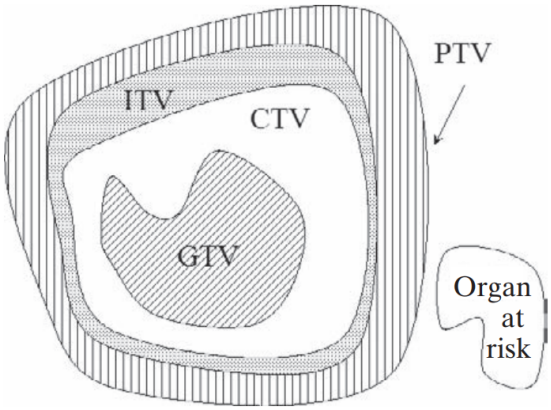

Figure 4: Graphical representation of target volumes and critical structures, as defined in ICRU Report No.50 and No.62[8].

2.4 Robustness

2.4.1 Robustness in photon-radiotherapy

With photon RT it can be assumed that the prescribed dose will be delivered to the CTV as long as CTV only moves within the delineated boundaries of the PTV. In that respect photon treatment plans have high *robustness* against the uncertainties incorporated into the PTV formalism. Robustness refers to two properties in the planning and delivering of a TP: Firstly, a robust TP ensures that the prescribed dose is delivered to the CTV despite potential uncertainties[22]. Secondly, a robust TP ensures that dose-level constraints of the OARs are to the best degree satisfied despite potential uncertainties. Potential uncertainties are the uncertainties defined in the optimization of the TP. Due to the physical properties of photons, photon RT optimized with the PTV-formalism and OAR constraints is "by itself" a robust dose-delivery technique.

2.4.2 Robustness in proton-radiotherapy

As protons are fundamentally different from photons the same PTV formalism and optimization techniques are not extensible to protons in order to ensure a robust dose to CTV and OAR sparing. For PT, dose distribution is greatly affected by the various uncertainties previously discussed in section 2.1. Additionally for PT, dose-distribution can be perturbed not only near the boundaries but also from within the target volume itself, a consequence from the steep dose gradients[9][22][23]. Hence, the PTV-formalism is less effective in ensuring target coverage for PT. With PT the impact on each individual beam due to the various uncertainties can vary significantly as each beam path can be greatly different, e.g. different in density-inhomogeneities or possible organ motion. This is the main idea the PTV-formalism fails to incorporate, since the same problem does not exist for photons.

As each proton beam requires lateral, distally and proximally margins to account for potential target displacements, a beam-specific planning target volume (BSPTV) is generated for each beam[25]. In addition, the range uncertainty introduced from the conversion of HU values into stopping powers is also incorporated in the creation of the BSPTV. The target displacement and range-uncertainty used in the creation of the

BSPTV is predetermined and can vary between diagnosis due to the difference in anatomical environment. For example, in the treatment for HL patients at the Skandion clinic, a symmetric 7 mm geometric displacement and a 4.5% range-uncertainty is used[7], which are based on study by Paganetti[24]. When creating a BSPTV the margins and uncertainties are applied around an already existing volume such as the CTV. Displayed in figure 5 is an example of two BSPTVs, represented by the red contours, from two different fields. In sharp contrast with the shapes of PTVs, BSPTVs can achieve highly asymmetric shapes around the CTV, e.g. like the "horns" seen in figure 5. These arise as a consequence because of how a small displacement of a few mm would significantly change the protons path near the edges of CTV, from air located in the lungs to normal tissue. As protons travel further in air than in normal tissue for a given energy the RO must take this into account, resulting in these "horns". However, it should be clarified that while a TP optimized with the PTV-formalism ensures that the PTV is treated adequately as the CTV, this is not the case with TPs optimized with RO, since such a requirement does not exist. Instead with PBS-PT the location of the pencil beam or spots are placed within the boundaries of the BSPTVs which means that the design of these field specific targets greatly influence the resulting target coverage and OAR sparing[25]. However, while spots **is** placed only within the BSPTVs it is not necessary to cover the whole of the BSPTVs and it is important to understand that the final spot location is determined at a later stage in the optimization process.

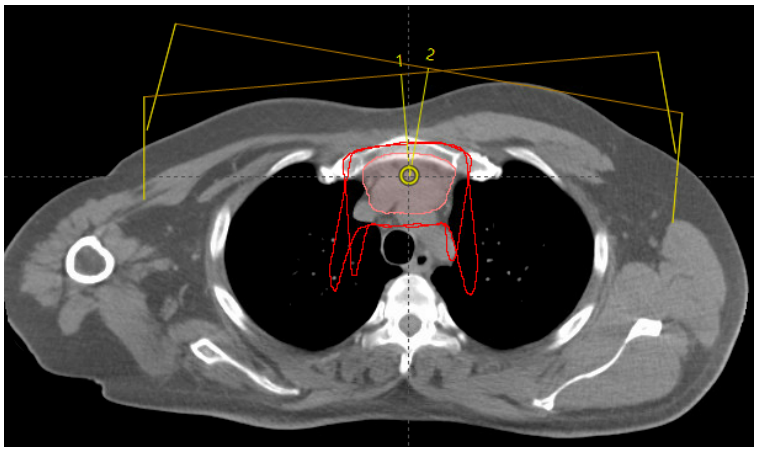

Figure 5: Two beam-specific planning target volumes (BSPTV), represented by the red lines, generated with a symmetric 7 mm geometric displacement and a 4.5% proton range-uncertainty, around the CTV (pink). BSPTVs created in EclipseTM treatment planning system (Varian Medical Systems, Milpitas, CA), from two anterior fields (1 and 2).

Similar to the pre-optimization defined BSPTV, potential uncertainty scenarios are defined in the optimization process with same and/or different margins as the BSPTV to further help the RO process and are referred to as perturbations[25]. Therefore, the generated perturbations looks the same as the BSPTVs, seen in figure 5. The optimizing process then utilize all the *defined* perturbations and optimize a dose plan with all scenarios simultaneously in consideration. These perturbations are what ultimately determines where spots are placed, not the BSPTVs. As such, margins in the RO-process are **scenario-based margins** which are different from the conventional geometric margins applied in the PTV-formalism and is an important distinction[26]. Incorporating the perturbations in the optimization process through where the optimizing algorithm is allowed to place spots, a TP which is less sensitive to the previously mentioned uncertainties can be created, i.e. a robust TP. Lastly, evaluation of TPs is performed by generating same/similar un-

certainty scenarios as used in the RO process and evaluating defined dose criteria, e.g. CTV $D_{98\%}$, with respect to generated dose distribution from all *defined* potential uncertainty scenarios. In summary, with robust optimization in RT dose criteria is applied on the CTV rather than the PTV (in contrast with the PTV-formalism) since RO ensures adequate target coverage and OAR sparing[25].

2.4.2.1 Robustness and proton therapy optimization techniques

If using multiple fields the robustness of a proton TP is also determined by the optimization technique utilized, with two common techniques being Single Field Uniform Dose (SFUD) and Multi-Field Optimization (MFO)[27]. With SFUD-optimization spot positions and weights (Monitor Unit (MU) per spot) are optimized independently for each beam, where each beam provides an uniform dose coverage over CTV. Consequently with the SFUD-optimization technique there is a limited ability to spare OAR located in the beamline. On the other hand with MFO spot positions and weights are simultaneously optimized in order to together achieve a homogenous dose distribution over CTV, i.e. dose distribution from each individual field can be greatly heterogeneous but the resulting dose coverage from all fields together is uniform. For complex geometries MFO is thus more effective than SFUD in reducing dose to OARs, however, as each field optimized with SFUD provides full coverage over CTV the resulting TP is generally less sensitive to uncertainties and therefore more robust than MFO TPs[27].

2.5 Treatment planning in Eclipse

The Eclipse treatment planning system (Varian Medical Systems, Milpitas, CA) (Ecplise^{TM}) is a widely used software for PT planning and is built on the features of the photon Ecplise^{TM}[25]. When optimizing a proton TP, beam angles are usually selected to have the least amount of density-inhomogeneity, least amount of normal tissue and as few OARs in the beam path as possible. In the first step of the RO-process, BSPTVs are created with desired margins and in Ecplise^{TM} the planner can themselves delineate BSPTV by using contour margin tools, however, more commonly used is the beam-specific target creation utility tool[25]. With this the planner define the margins associated with each uncertainty defined in the RO process, e.g. "Positioning Uncertainty" (set-up error), "Axial Uncertainty"(range uncertainty).

Before TP-optimization the planner must define target margins for each beamline by utilizing the BSPTVs. A treatment plan is thereafter optimized with inverse planning where a desired dose distribution is provided by minimizing an objective function based on dose volume constraints specified in the optimization[25]. These include upper and lower dose-objectives placed on e.g. CTV and OAR to steer the optimizer in desired direction. Before optimization, an optimizer-algorithm and calculation model must be chosen, e.g. the Nonlinear Universal Proton Optimizer (NUPO) and the Proton Convolution Superposition (PCS). Within the optimizer "Perturbations" are defined with similar uncertainties as for the BSPTV creation. These perturbations incorporate the associated uncertainties with PT in the optimization process itself, i.e. RO, such that a TP less sensitive to these can be created. These perturbations are what ultimately determines where spots are placed by the optimizer. Each perturbation can result in different dose-distributions and the optimizer can visualizes these by computing the maximum and minimum dose value received by delineated contours from all defined perturbations. Additionally in the optimizer, "Normal Tissue Objective" (NTO) can be defined which determines constraints on normal tissue not represented by OARs.

2.6 Image Registration

Image Registration (IR) is an important tool as it allows for the registration/interconnection between imaging data acquired, e.g. at different times (i.e. multi-temporal) or from different imaging devices (i.e. multi-modality). This is important when evaluating TPs on vCTs as delineated contours from the pCT must be transferred to the vCTs. For this purpose IR is essential as it is not always true that a pixel/voxel located on a given coordinate among the images represent the same anatomical structure, regardless of that the images are aligned with a reference coordinate. In summary this is the issue IR needs to resolve. This is achieved by finding the spatial correspondence transform which minimize the difference between the images[28]. For example, consider two sets of images, a source image F(x) (also referred to as the fixed image) and the target image M(x') (also defined as the moving image). The IR algorithm estimates the best spatial correspondence transform, T(x'), which minimize the difference between the source image and target image. T(x') is derived as the sum of all local position vector in the target image, i.e. x', and the displacement vector between the images, i.e. $\mathbf{u}$(x'). Thus IR can be defined as:

$$F(x) = M(T(x')) = M(x' + \mathbf{u}(x')) \ . \tag{2}$$

2.6.1 Rigid and non-rigid image registration

IR can be categorized as two types: Rigid and non-rigid, i.e. Deformable Image Registration (DIR). With Rigid Image Registration (RIR) the spatial correspondence transform is limited to a uniform rotation and translation where all pixels move and rotate uniformly with six degree of freedom (Rotation, Pitch, Roll, Vertical, Longitudinal and Lateral)[28]. Consequently, the pixel-to-pixel relationship of every pixel in the source image and target image will remain the same before transformation and after.

In cases where no anatomic change is expected RIR is an effective and sufficient registration method, however, RIR cannot handle anatomical structural changes between images, because the pixel-to-pixel relationship of every pixel in the source image and target image will be the same before transformation and after[28]. In comparison, with DIR the pixel-to-pixel relationships can change, resulting in a "deformed" image. DIR has a higher degree of freedom as well as a non-uniform rotation and translation of the pixels which means local distortions between image sets can be managed (i.e. anatomical structural changes). One application for which DIR is used is when transferring contours delineated on one image study to another, e.g. from a pCT to vCTs acquired during treatment. The DIR can match the two anatomies, deforming the contours with respect to the local distortions between the image sets, allowing for a better representation of the patient's anatomy. It is important to note that the DIR can manage local distortions but its accuracy worsen with an increasing distortion, suggesting that large distortions cannot be deformed to a high precision[28]. Vickress et al [19] concluded that large displacements is typically distortions larger than 20 mm, highlighting that the DIR algorithms' performance must be individually evaluated for each patient.

The way any DIR algorithm connects voxels from the source image to voxels in the target image is through a Deformation Vector Field (DVF), where the DVF directly describes the correspondence between the source and target image[19][28]. The DIR algorithm is characterized partially by the approach at which the DVF is generated. All algorithms consist of three components: Regularization, Image Similarity Metric (ISM)

and Optimization. Regularization describes how the algorithm based on desired properties, e.g. gradients in image intensity value or conservation of continuity or mass, generates a realistic DVF. A comprehensible, illustrative representation of DVF is by using arrows which size and direction represents the magnitude of deformation and direction (see figure 6C). The next component in the DIR algorithm, the ISM, defines how "veracious" the image registration is. Lastly the Optimization describes how the algorithm combines the Regularization and Image similarity metrics to optimize and reach an optimal DVF. In figure 6 a schematic illustration of DIR is displayed. Figure 6A represents the source image, 6B the target image, 6C the generated DVF and 6D the resulting deformed image and contour. Between A and B the shape changed from a rounded boundary in A into a boundary with four sharp corners in B, in analogy with anatomic changes between pCT and vCTs. The produced DVF makes it clear that the largest magnitude of deformation is observed at the corners and gradually decreases, which agree with the difference observed between image A and B. Lastly the DIR locally deforms the four sharp corners to produce the contours seen in figure 6D.

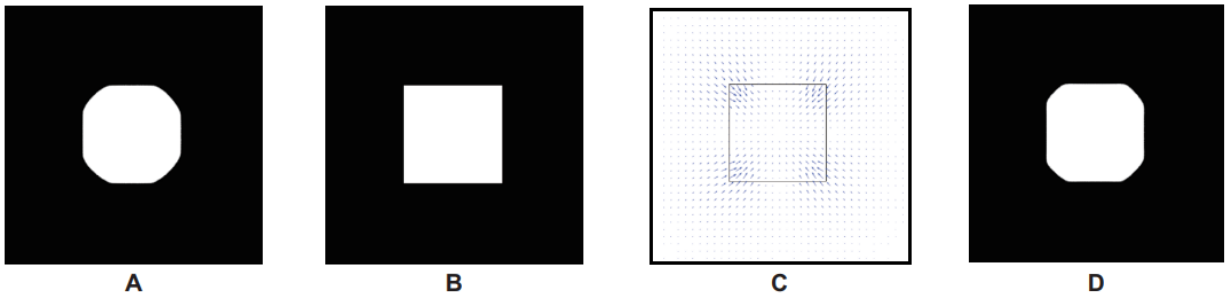

Figure 6: Illustrative representation of the Deformable Image Registration process. A represents the fixed image and B the moving, while C is the generated deformation vector field used to produce the deform image D[28].

2.6.2 Similarity metrics

Contours (e.g. CTV and OARs) delineated on medical images, are often compared in order to evaluate contours or the performance of an image registration. These types of measurements, where two datasets of points are compared, can be categorized with respect to how the individual point in the data set is considered. Two such categories are the *Overlap based measures* and *Spatial distance based measures*[29].

2.6.2.1 Dice Similarity Coefficient

The Dice Similarity Coefficient (DSC) is an example of an Overlap based measure where the overlap (intersection) between two regions, e.g. X and Y, is quantified. DSC is calculated as:

$$DSC = \frac{2 \cdot X \cap Y}{X + Y} \quad , \tag{3}$$

where the number of shared pixels/voxels between the two regions, $X \cap Y$, times two is divided by the total number of pixels/voxels of set X and Y. A perfect overlap would yield a DSC value of 1 while no overlap would yield DSC equal to 0. A schematic illustration of DSC is displayed in figure 7. One drawback of overlap based measurements is that it is only the intersection between the two sets which are important, the position of individual points are irrelevant, i.e. it makes no difference where a point is located only if it is in the intersection or not. Overlap measurements are therefore generally less sensitive to outliners.

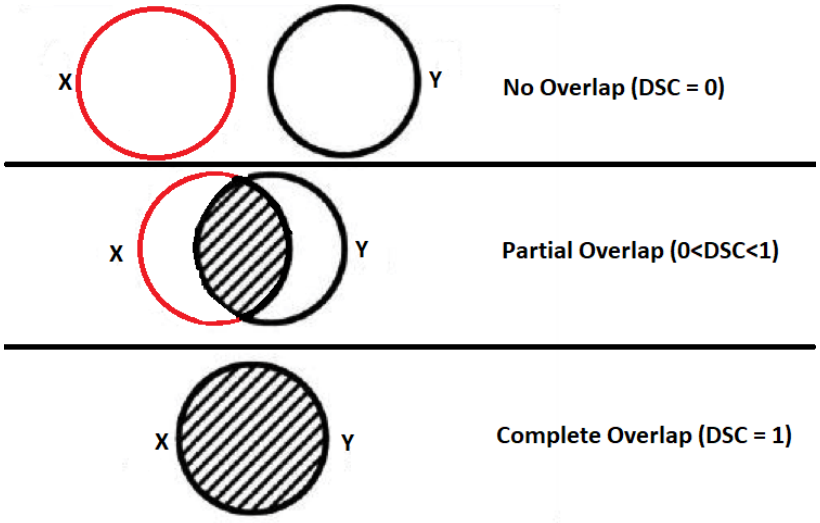

Figure 7: A schematic illustration of DSC.

2.6.2.2 Hausdorff Distance

In some instances the overlap between two regions is not sufficient or required and it is instead the spatial position of the points which are important. If that is the case, spatial distance based measurements, where the pairwise distances between two regions is computed, can be utilized. The max-min distance between two regions can be quantified with the Hausdorff distance (HD), which represent the largest distance between the two datasets. Consequently, with spatial distance based calculations the spatial position of every point is taken into consideration which inevitable makes it sensitive to outliners[29]. The directed Hausdorff distance $\hat{H}(X,Y)$ for point-set X and Y is given by the maximum distance between any point $x \in X$ to its nearest neighbor in $y \in Y$ and vice-versa, i.e.:

$$\hat{H}(X,Y) = \max_{x \in X} \left(\min_{y \in Y} (d(x,y)) \right) \ , \tag{4}$$

$$\hat{H}(Y,X) = \max_{y \in Y} \left(\min_{x \in X} (d(y,x)) \right) \ , \tag{5}$$

where $d(x,y)$ and $d(y,x)$ is the euclidean distance between point x and y. The directed Hausdorff distance is not symmetric since it is not given that $\hat{H}(X,Y) = \hat{H}(Y,X)$. A schematic illustration of the directed Hausdorff distance is displayed in figure 8. Hence HD is defined as the maximum directed Hausdorff distance in either direction, i.e. either $X \to Y$ or $Y \to X$, given by:

$$\text{HD} = \max \left(\hat{H}(X,Y), \hat{H}(Y,X) \right) \ . \tag{6}$$

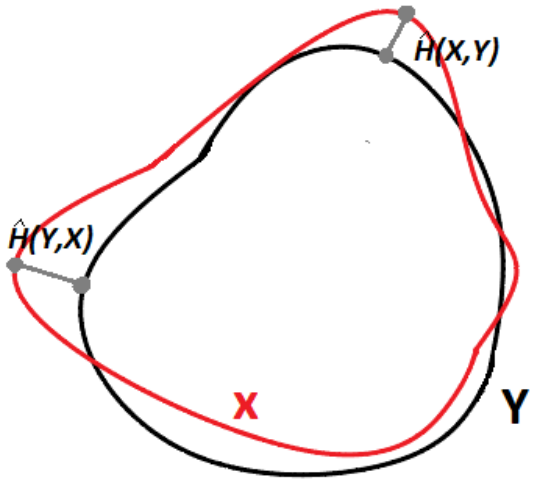

Figure 8: A schematic illustration of the directed Hausdorff distance for set X and Y.

2.7 PT treatment at the Skandion clinic

PT treatment in Sweden is given at the Skandion clinic with a PT system from Ion Beam Applications (IBA) (Proteus Plus, IBA, Louvain-la-Neuve, Belgium), one of the major manufacturer of PT systems. The PT application at the Skandion clinic utilizes the PBS beam delivery technique and can produce protons with energies of up to 60-230 MeV. Additionally, for superficial tumors, the beams' energy can be degraded with a range shifter, where the range shifter is inserted perpendicular to the beam-line at the beam-delivery "head"[30].

All preparations before treatment at the Skandion clinic such as: fixation, planning CT-acquisition, DIBH-evaluation, target delineation and dose-planning are performed at the patients "home" university hospital. When patients arrive at the Skandion Clinic some time will have passed since the acquisition of the pCT (CT image acquired at the home university hospital). Hence, before treatment start, a vCT is acquired and evaluated with respect to the same parameters as the pCT. Incorporating vCTs within the treatment is an important step in ensuring sufficient target coverage and adequate OAR sparing throughout treatment (see section 2.2). In addition, contours delineated on the pCT are transferred to the vCTs by using RIR. At the Skandion clinic, vCTs are acquired at least once a week for most treatments. Since 2020 some of these vCTs have been acquired with a low dose protocol (4-5 times lower dose than the normal protocol), and it has been verified by the Skandion clinic that this does not influence the dose calculation accuracy.

2.7.1 PRO-Hodgkin study

There is an ongoing study (2019-), the "PRO-Hodgkin: Clinical investigation of PBS proton treatment in Hodgkin lymphoma patients" (PRO-Hodgkin), which rationale is to demonstrate the physical and dosimetric advantages with PBS proton therapy for treatment of HL. Recurrence, survival rates and side-effects for patients diagnosed with HL, treated with PBS-PT, will be compared to a control group which received photon-radiotherapy between 2009-2013. Patients included are those who meet the studies inclusion criteria, which can be found in the study protocol[3]. Furthermore, PRO-Hodgkin is a national collaboration between

the seven university hospitals in Sweden. The number of patients receiving PT for HL during the five-year study period which will be included in the study is estimated to be at least 75 patients from all seven university hospitals. Dose volume objectives and constraints defined in the PRO-Hodgkin study are presented in table 1.

Table 1: Dose volume objectives and constraints given in biological dose for the PRO-Hodgkin study. L- and R-Breast indicates either left and right breast.

Volume	Objectives/constraints in biological doses Gy(RBE)
CTV	$D_{98\%} \geq 95\%$
Heart	D_{mean} as low as possible $V_{15Gy(RBE)}$ as low as possible
LungTotal	D_{mean} as low as possible $V_{5Gy(RBE)} < 55\%$ $V_{20Gy(RBE)} < 30\%$
L Breast and R Breast (women $<$ 30 years)	D_{mean} as low as possible $V_{5Gy(RBE)}$ as low as possible
Esophagus	$D_{2\%}$ as low as possible

3 Material and Method

In this section, the patient-cohort is first described followed by a description of the three distinct parts conducted in this thesis. The first part consisted of an evaluation of the IR technique used to transfer contours from the pCT to the vCTs acquired during the treatment course. Thereafter, the original TPs were investigated to determine if smaller margins in the RO-process could be possible. Lastly in part 3, the robustness and OAR sparing of TPs with smaller perturbations applied in the RO-process were evaluated.

3.1 Patient data

The patients included in this thesis are patients diagnosed with HL who received PT treatment with DIBH at the Skandion clinic through Skåne University hospital as their home clinic. As such, all CT images were acquired following clinical practice. Furthermore, only a CTV-expansion contained in the anterior thorax region was included. Nine patients were included in this study and detailed characteristics of the patient-cohort including CTV volume, prescribed dose, optimization technique and spot-spacing used are provided in table 2. However, patient 7-9 were included at a later stage in the study and therefore only partially included in part 2, but completely in part 3. The research material for this study consisted of contours delineated on pCTs, *treatment approved* dose-plans and acquired vCTs at the Skandion clinic.

Table 2: Patient plan characteristics.

Patient	CTV volume [cm^3]	Dose [$Gy_{(RBE)}$]	Optimization technique	Spot-spacing [cm]
1	130	29.75	SFUD	0.5
2	73	20.00	SFUD	0.5
3	367	29.75	SFUD	0.5
4	126	29.75	SFUD	0.5
5	169	36.00	SFUD	0.5
6	169	29.75	SFUD	0.5
7	311	29.75	SFUD	0.5
8	168	29.75	SFUD	0.3
9	144	29.75	MFO	0.3

3.2 Part 1: Image Registration

Each patient had a pCT acquired at Skåne University Hospital, as well as 2-4 vCTs acquired at the Skandion Clinic during their treatment. Contours from the pCT were transferred to the vCT through IR with Eclipse^{TM} treatment planning system (Varian Medical Systems, Milpitas, CA). The RIR in Eclipse^{TM} utilizes a six degree of freedom (see section 2.6), while the DIR is based on the accelerated Demons algorithm, which drives the IR by using the gradients in image intensity values[19]. The source image was the pCT image and the target image was the vCT images. As the vCT contains information about anatomical deviations from the initial pCT image, DIR was used to deform the contours. It was hypothesized that transferring contours with DIR instead of RIR would generate contours which better represent the *current* anatomical state of the patient in comparison with RIR. However, in order to perform a DIR the two images need to be located in the same coordinate system, i.e. a RIR was first performed. Additionally, the RIR maximizes the overlap between the images, improving the DIR performance since it is most efficient at deforming local deviations.

RIR was performed by placing a Volume of Interest (VOI) around the anatomy/structures which the RIR would base the registration on and as the RIR algorithm register images through the value in each voxel, one can choose which values the RIR should base its IR on. In order to mitigate uncertainties associated with IR based on soft tissue, the voxel value related to bones (which in a CT-image corresponds to HU 200-1700), was used. As CTV was located in the anterior thorax region, every VOI for each RIR (one per vCT) was placed around sternum including some bone structures. The RIRs were visually verified to be "as good as possible", which basically meant that the bones between the images aligned well. Perfect alignment is not possible between different scans due to small variations in set-up. This problem was mitigated by only registering on sternum and nearby bone structures, which means that the registration will worsen gradually in the posterior direction. However, this will be ignored since the region which had a "bad" alignment received no/low dose in the original dose plan. Thereafter a DIR was performed to deform and transfer delineated contours from the source image, i.e. pCT, to the moving image, i.e. vCT. This was performed on every vCT acquired for each patient. Contours transferred were CTV, heart, combined volume of left and right lung (referred to as LungTot), esophagus and left and right breast for the female patients. Contours were also transferred based on the RIR (henceforward referred to as RIR Sternum) in order to evaluate the performance of the two IRs in generating accurate representations of the underlying anatomy.

3.2.1 Evaluation of the Image Registration

To be able to use the DIR generated contours for dose comparisons in this study, it was important to evaluate the performance and accuracy of the IR used. However, the lack of quantitative validation in image registration and contour segmentation constitutes one of the key challenge in these types of studies. Similar to other studies[31][32][33], the accuracy of the generated DIR contours was evaluated solely based on visual inspection. The visual inspection was performed by a physician, who evaluated both the deformable contours and the rigid ones based on how well they represented the underlying *true* anatomy. Each contour was graded as follow:

1. The generated contour is clinical acceptable and require **no** modification.
2. The generated contour is clinical acceptable after **minor** modification.
3. The generated contour requires **major** modification before they can be clinical accepted (i.e. they are unacceptable).

If a deformable structure received assessment "2" or "3" the physician was asked to perform the necessary correction such that the contour could be considered clinically acceptable. However, the physician concluded that contours receiving assessment "2" would still be clinically acceptable regardless of the minor deviation in representing the underlying anatomic volume. Thus, only deformable contours graded as "3" would be corrected. Furthermore, contours generated from the rigid registration were only evaluated, **not** corrected, since these contours were not used further in the study. Henceforward, the RIR and DIR contours will not be distinguished and the following measurements only considers the DIR generated contours.

3.3 Part 2: Evaluation of the original treatment plan

The analysis of the original plan consisted of a geometric and dosimetric evaluation. For the geometric analysis, the contours from the pCT were compared with the deformed contours from the vCTs by evaluating volume deviations seen for total lung volume and CTV. Hausdorff distances were also computed. This was followed by a dosimetric evaluation where the original TPs were recalculated on the vCTs and Dose-Volume-Histogram (DVH) parameters were computed.

3.3.1 Geometric analysis

3.3.1.1 Volume evaluation

An important factor in ensuring a robust dose to CTV and robust OAR-sparing with DIBH during proton treatment is the patient's ability to reproduce their DIBH at every fraction. Evaluation of the reproducibility (see section 2.7.1) includes the variation of lung volume during various breath-holds, as such the total lung volume (LungTot) throughout the image series (pCT + vCTs) was recorded and evaluated. In addition volume variation of CTV was also investigated. These volumes were evaluated by computing the relative deviation in volume between each vCT with the same structure from the pCT.

3.3.1.2 Hausdorff distance calculations

The Hausdorff distance (see section 2.6.2), was calculated to establish an overview of the extent of margin required for each planning CTV in order to cover each deformed CTV contour throughout treatment. The HD was determined for each patient by comparing the planning CTV with respective verification CTV (deformed CTV) and for these computations Python(Ver 3.2.6) was used. However, the planning CTV and respective deformed CTVs were located in different CT-image series which meant that it is not necessarily true that a pixel/voxel located on a given coordinate among the images represents the same anatomical structure. HD calculations could thus not directly be performed by comparing a planning CTV located within pCT with a deformed CTV located within vCTs. In order to circumvent this problem each deformed CTV were propagated to the pCT with the RIR Sternum performed earlier. It is therefore the accuracy of the RIR algorithm which determines the uncertainty for these calculations.

In addition, equation 4-6 is applicable on two dimensional data-sets, however, the structure sets represents three dimensional objects which means that the HD must be determined slice-wise. With sternum as reference point, the HD was computed in three orientations: Superior-Inferior (SI), Left-Right (LR) and Anterior-Posterior (AP). A schematic illustrative figure clarifying these orientations is presented in figure 9. Furthermore, the location of the slice in figure 9 represents "Slice 0", i.e. the origin. Thus HD was determined slice-wise, in three directions for each vCT of every patient. Thereafter the maximum HD value from all the vCT were recorded and evaluated for patient 1-6.

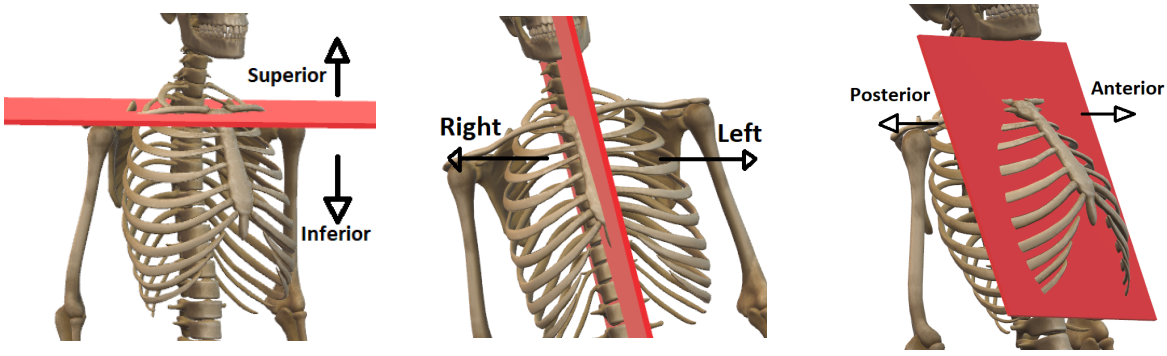

Figure 9: Three orientations for which the Hausdorff distance was determined at. The red slice represents the origin, chosen as the slice which passes through upper sternum.

3.3.2 Dosimetric analysis

One limitation of any geometric evaluation is the effect the metrics observed will have on the resulting dose distribution, i.e. there is a lack of connection between observed geometrical error and resulting dosimetric error[34]. For this reason part 2 of this study also consisted of a dosimetric analysis, evaluating dose-distribution changes between the pCT and the vCT with the deformed contours. The first step was transferring the original plan from the pCT to the vCT. A RIR is required for this transfer and once again the same RIR as previously, the RIR Sternum, was used for all patients. Thereafter the original plan was recalculated on every vCT and DVH parameters were acquired. The same dose-calculation algorithm, PCS Version 15.6.04, was used for all TPs.

The DVH parameters examined were in accordance with the guidelines given by the Pro-Hodgkin study (see section 2.7.1, table 1). Each DVH parameter was evaluated with respect to the deviation in dose between the pCT and vCTs, except $D_{98\%}$ for CTV where the absolute value was evaluated. Additionally, the order in which the vCTs were acquired was distinguished to determine any possible trend throughout treatment. It should be clarified that patient 3, due to large variations in DIBH reproducibility, received a new treatment plan after the second vCT had been acquired, i.e. the original plan was not delivered throughout the treatment. However, from this thesis perspective the dose deviations from the original plan if delivered on the last vCT is still relevant and were therefore included in the dosimetric analysis.

3.4 Part 3: Treatment plans with smaller margins

3.4.1 Optimization of treatment plans

From the previous parts a tendency to possibly utilize smaller margins in the RO-process, which would still ensure a robust dose to CTV and robust OAR sparing, was observed. As discussed in section 2.4.2, the margins used in the RO-process are **scenario based margins** (defined as perturbations), not conventional geometric margins, and as such smaller margins refers to smaller perturbations in the RO-process. In accordance with the proton treatment planning method at Skåne University Hospital, the margins used in the RO-process, i.e. perturbations, for each patient were a symmetric 7 mm geometric displacement and a 4.5% proton range-uncertainty. For each patient, three new TPs with smaller perturbations were investigated: One with a symmetric 5 mm geometric displacement and a 4.5% range-uncertainty, one with a symmetric 3 mm geometric displacement and a 4.5% range-uncertainty and one with a symmetric 5 mm geometric displacement and a 3.5% range-uncertainty. These were referred to as: **P1 5mm 4.5**%, **P2 3mm 4.5**% and **P3 5mm 3.5**% with the original plan defined as **P0 7mm 4.5**%. The smaller margins in the BSPTV creation and in the RO-process were the only changes from the original TPs and all other parameters were kept the same as much as possible.

All TPs were created in EclipseTM as discussed in section 2.5, which was the same software the original TPs were created in and each TP was created as in clinical practice. First a copy of the original plan with the original pCT was made such that the new plans had the same number of fields, same field angle and snout position as the original plan. Thereafter a BSPTV was created for each field with the beam-specific target creation utility tool. Only "Positioning Uncertainty", i.e. set-up error, and "Axial Uncertainty", i.e. range uncertainty, were changed between the plans at this step. Target margins were then defined for each beamline and same margins were used as in the original plan.

Optimizer-algorithm and calculation model used in the treatment planning were the NUPO (Version 15.6.03) and PCS (Version 15.6.04) and all settings within these were identical to the original plan. Perturbations were defined in the optimizer with the same uncertainty margins as for the BSPTV creation as mentioned in section 2.5. A common practice at Skåne University hospital is also defining additional perturbations with smaller setup uncertainties. The perturbations used for each TP are provided in table 3. Additionally, for all TPs the same NTO settings as in the original plan were used. Lastly, all TPs were optimized with the same dose volume constraints as the original plan. However, to consider all TPs with smaller margins clinically acceptable, the maximum dose was kept below 110% of the prescribed dose and the number of MU/spot did

not exceed the value in the original plan. Therefore, on some TPs additional dose volume constraints, e.g. constraints on 105% isodose volume, were used in the RO-process. All TPs, including the original TPs, were robust evaluated as described in section 2.3, by generating various uncertainty scenarios (table 3). As given in the Pro-Hodgkin study 10 out of 12 perturbed dose distributions should reach the dose criteria for CTV $D_{98\%}$, i.e. $D_{98\%} \geq 95\%$.

Table 3: Perturbations and uncertainty scenarios defined in the robust optimization process and for the robust evaluation of each treatment plan..

Treatment plan	Perturbations	Uncertainty scenarios
P0 5mm 4.5%:	7mm 4.5%	7mm 4.5%
	5mm 4.5%	5mm 4.5%
	3mm 4.5%	
P1 5mm 4.5%:	5mm 4.5%	7mm 4.5%
	3mm 4.5%	5mm 4.5%
P2 3mm 4.5%:	3mm 4.5%	7mm 4.5%
		5mm 4.5%
		3mm 4.5%
P3 5mm 3.5%:	5mm 3.5%	7mm 4.5%
	3mm 3.5%	5mm 4.5%
		5mm 3.5%

3.4.2 Dosimetric analysis of treatment plans with smaller margins

Similar to the dosimetric analysis conducted in part 2, CTV $D_{98\%}$ was determined at each vCT for all treatment plans to validate the robustness of these plans. DVH parameters, same as in part 2, were acquired for all TPs as well as the $D_{95\%}$ isodose volume size.

4 Results

4.1 Part 1: Image Registration

The result of the visual evaluation for the rigid and deformed contours, based on criteria presented in section 3.2.1, is displayed in table 4.

Table 4: Result of the visual evaluation for the rigid (4a) and deformed contours (4b), based on a grading scale of 1-3, where "1" represent no need for modifications of contours before clinical acceptance, "2" minor modifications and "3" major modifications. Contours which received grade "2" has been marked orange while contours evaluated with grade "3" have been marked red.

4a: Rigid contours

RIR Contours	Patient 1		Patient 2		Patient 3			Patient 4			Patient 5				Patient 6		
VerCT Nr	1	2	1	2	1	2	3	1	2	3	1	2	3	4	1	2	3
CTV	1	1	1	1	1	3	2	1	1	1	1	1	2	2	2	2	2
Heart	1	1	2	2	2	3	3	1	1	2	2	2	1	2	2	3	2
LungsTot	2	2	1	3	3	3	3	2	3	3	2	3	3	3	3	3	3
Esophagus	1	1	1	2	1	2	2	1	1	1	1	2	2	2	2	1	1
Breast	-	-	1	1	2	2	1	1	1	1	-	-	-	-	2	2	2

4b: Deformable contours

DIR Contours	Patient 1		Patient 2		Patient 3			Patient 4			Patient 5				Patient 6		
VerCT Nr	1	2	1	2	1	2	3	1	2	3	1	2	3	4	1	2	3
CTV	1	1	1	1	1	1	1	1	1	1	1	1	1	1	1	1	1
Heart	1	1	1	1	1	1	1	1	1	1	1	1	1	1	2	2	1
LungsTot	1	1	1	1	1	2	2	1	1	1	1	1	1	1	1	1	2
Esophagus	1	1	1	1	1	1	1	1	1	1	1	1	1	1	1	1	1
Breast	-	-	1	1	1	1	1	1	1	1	-	-	-	-	1	2	1

An extreme case of when the rigid contours required major modifications is presented in figure 10, where the rigid and deformable contours (LungTot and heart) from the same patient is displayed.

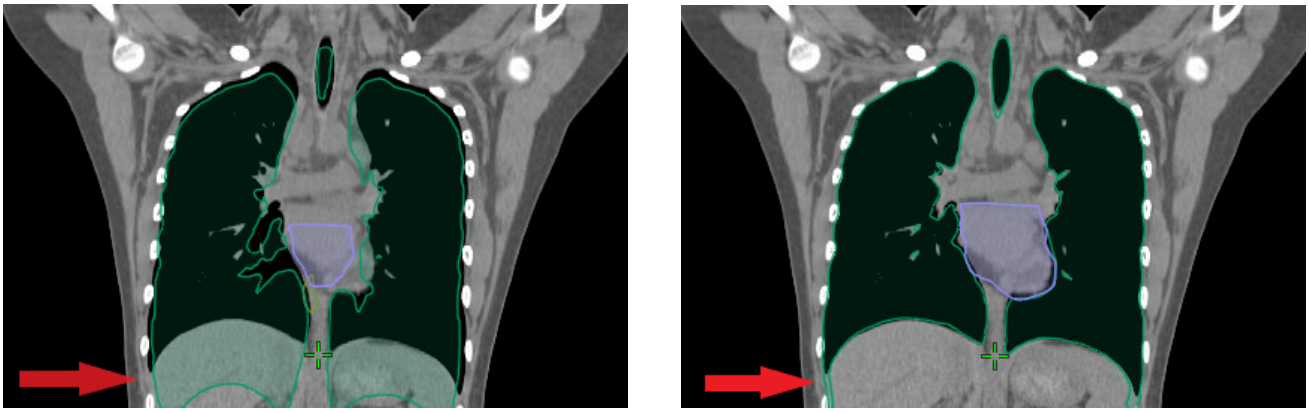

(a) Rigid contours (b) Deformable contours

Figure 10: Illustration of rigid (a) and deformable (b) LungTot and heart contours for the same patient. LungTot is displayed in dark green while the heart is displayed in purple. The red arrow highlights the overlap of the rigid LungTot contour and normal tissue and the absence of overlap with the deform contour.

4.2 Part 2: Evaluation of the original treatment plan

4.2.1 Geometric analysis

4.2.1.1 Volume evaluation

The lung volume deviation and the CTV volume deviation between each vCT deformed contour with the same structure from the pCT is displayed in figure 11 for all nine patients.

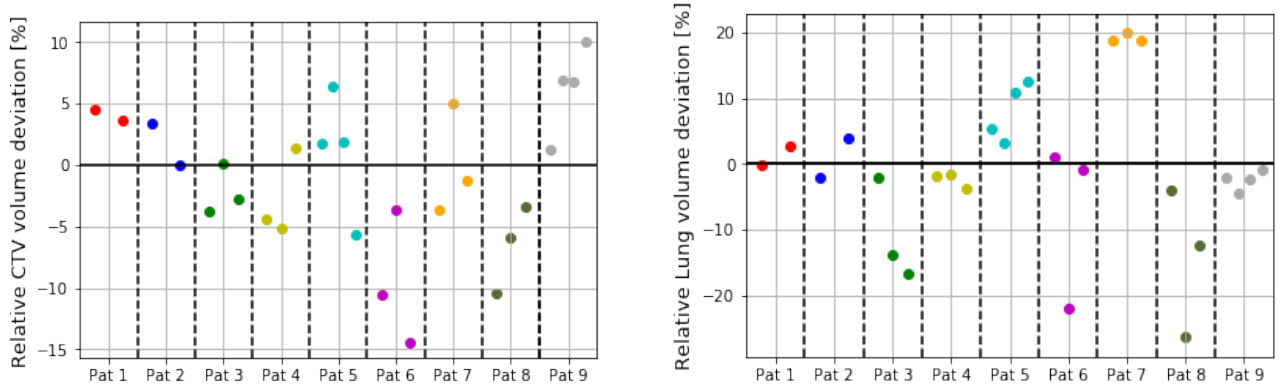

(a) CTV (b) LungTot

Figure 11: Relative CTV volume (a) and total lung volume (b) deviation between each vCT deformed contour with the same structure from the pCT. Black line represents zero volume variation. The colored points represents the relative deviation at each vCTs. Additionally, the first acquired vCT is the one furthest to the left, with the second one thereafter etc.

4.2.1.2 Hausdorff distance

The maximum distance between the total CTV volume from the vCTs and the pCT determined for patient 1-6 with the HD formalism, equation 4-6, is displayed in figure 12 for three different orientations.

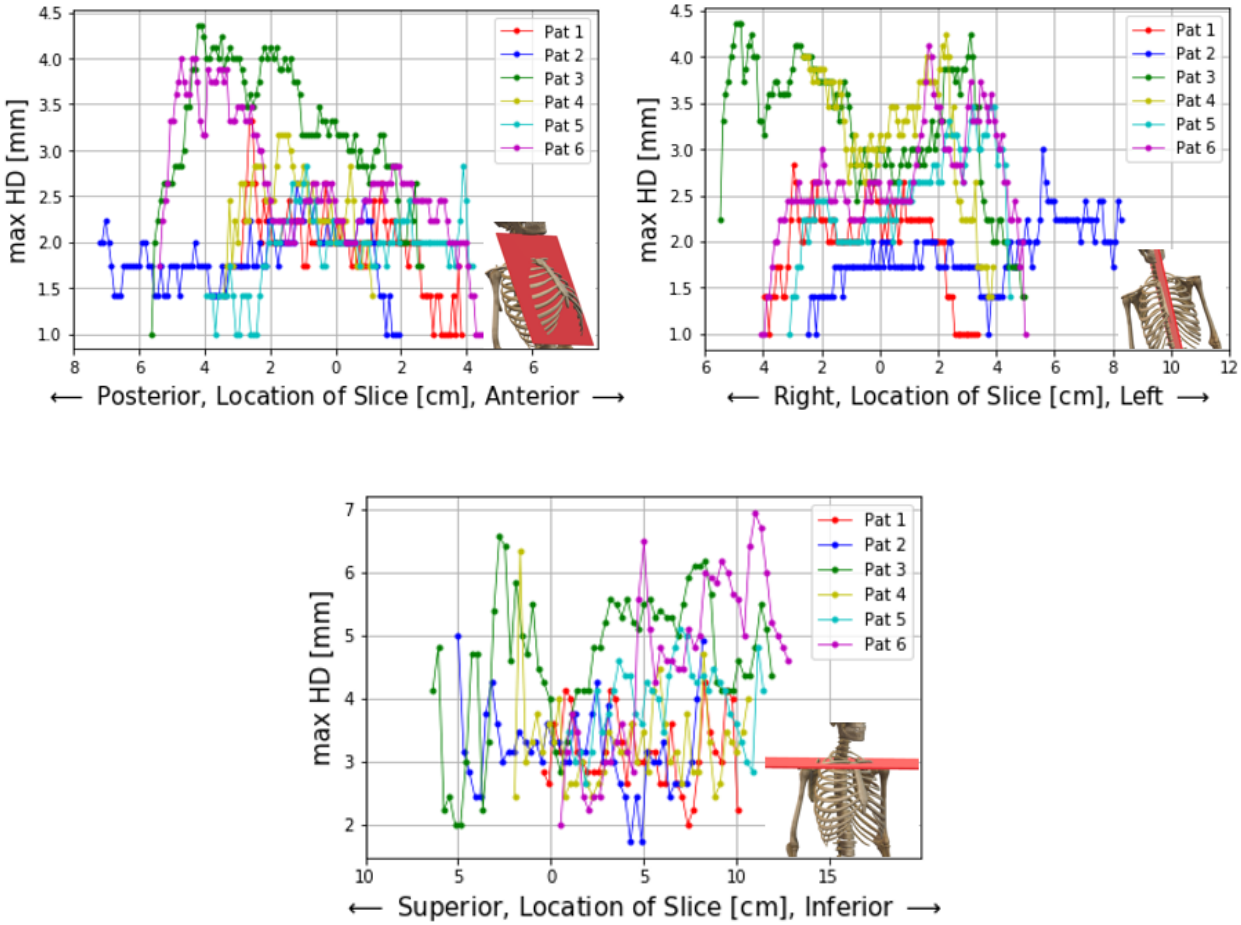

Figure 12: Hausdorff distance determined in three orientations for the planning CTV and the deformed contours. In each orientation the maximum HD is constructed slicewise, with slice "0" defined as the slice which passes through upper sternum. Furthermore, the x-axis describes the location of each slice with respect to slice "0". The HD calculations within one orientation describes motion in the other two orientations.

4.2.2 Dosimetric analysis

The dosimetric analysis of the original TPs, in accordance with table 1 for each patient, is displayed in figure 13-17, with CTV, heart, lungTot, esophagus, and left and right breast, respectively. Throughout all figures the black points represents the DVH parameters at the pCT, while DVH parameters for the deformed contours on the vCTs are represented by colored points. Additionally, as in section 4.2.1, the x-axis represents a time axis for the colored points where the first acquired vCT is the one furthest to the left and so on. Lastly, all DVH parameters except CTV $D_{98\%}$ were evaluated with respect to the deviation in dose between the pCT and vCTs, where zero dose deviation relative the pCT is represented by the black line. The actual dose or dose volume metrics which the patient received at the pCT is presented in table (5-8) for respective OAR after each figure.

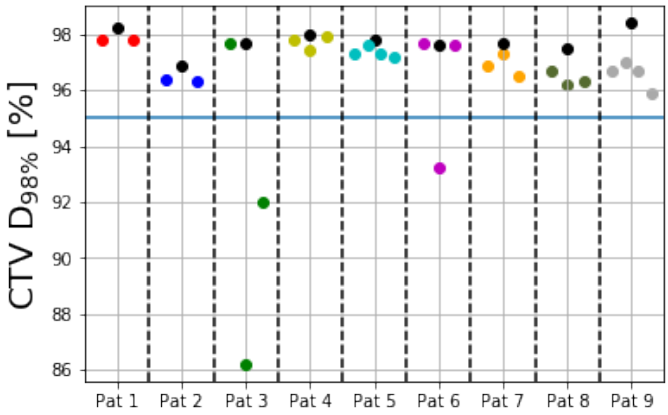

Figure 13: CTV $D_{98\%}$, where the black points represents CTV $D_{98\%}$ from the planning CT and the colored ones CTV $D_{98\%}$ received at the verification CTs. The blue line is the dose criteria for CTV $D_{98\%}$, i.e. CTV $D_{98\%} \geq 95\%$.

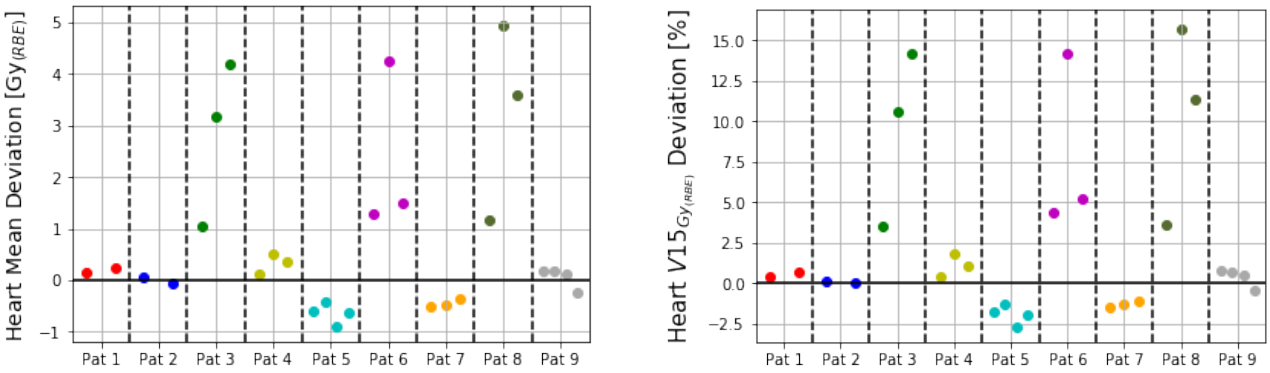

(a) Heart D_{mean}

(b) Heart $V_{15\text{Gy}_{(RBE)}}$

Figure 14: Heart D_{mean} (a) and absolute $V_{15\text{Gy}_{(RBE)}}$ (b) deviation from the planning CT for respective verification CT.

Table 5: Heart D_{mean} and the $V_{15\text{Gy}}$ determined from planning CT for each patient.

planCT	Pat 1	Pat 2	Pat 3	Pat 4	Pat 5	Pat 6	Pat 7	Pat 8	Pat 9
Heart D_{mean} [$\text{Gy}_{(RBE)}$]	0.8	0.3	4.0	3.3	4.5	4.3	3.1	6.2	1.0
Heart $V_{15\text{Gy}_{(RBE)}}$ [%]	1.0	0.0	12.1	9.8	12.9	14.3	9.0	18.9	1.1

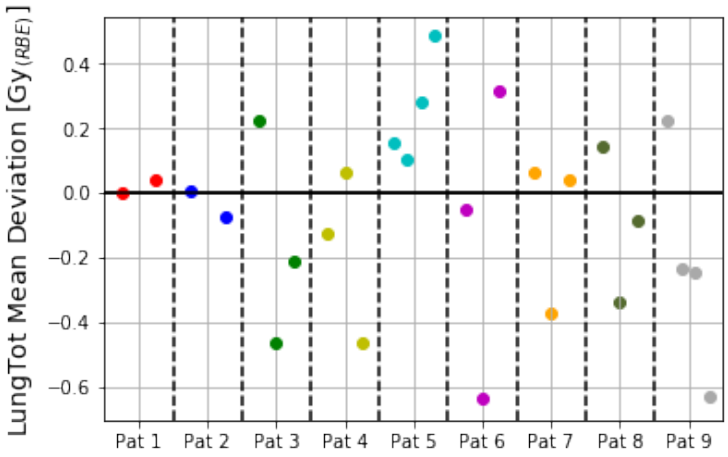

(a) LungTot D_{mean}

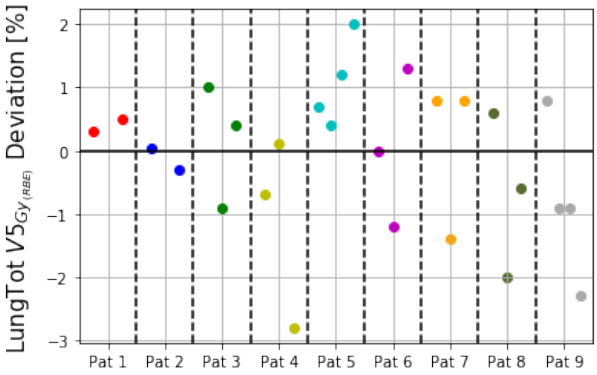

(b) LungTot V_{5Gy}

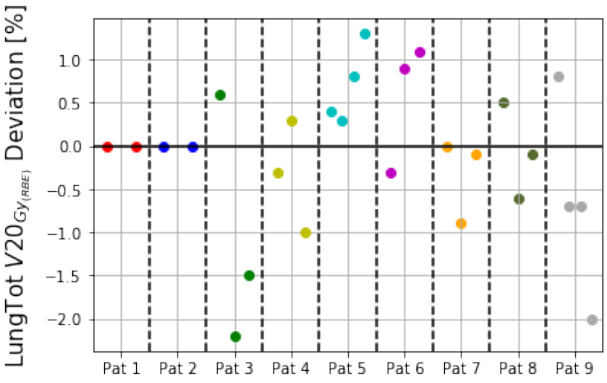

(c) LungTot V_{20Gy}

Figure 15: LungTot D_{mean} (a) and absolute LungTot $V_{5Gy_{(RBE)}}$ (b) and $V_{20Gy_{(RBE)}}$ (c) deviation from the planning CT for respective verification CT.

Table 6: Lung D_{mean}, $V_{5Gy_{(RBE)}}$ and $V_{20Gy_{(RBE)}}$ determined from planning CT for each patient.

planCT	Pat 1	Pat 2	Pat 3	Pat 4	Pat 5	Pat 6	Pat 7	Pat 8	Pat 9
LungTot D_{mean} $[Gy_{(RBE)}]$	0.7	1.2	5.1	3.1	2.9	2.8	3.3	3.4	3.2
LungTot $V_{5Gy_{(RBE)}}$ [%]	4.2	8.5	24.7	17.2	13.9	14.8	7.8	17.2	14.0
LungTot $V_{20Gy_{(RBE)}}$ [%]	0.0	0.0	13.8	6.2	6.2	6.5	15.9	7.1	8.5

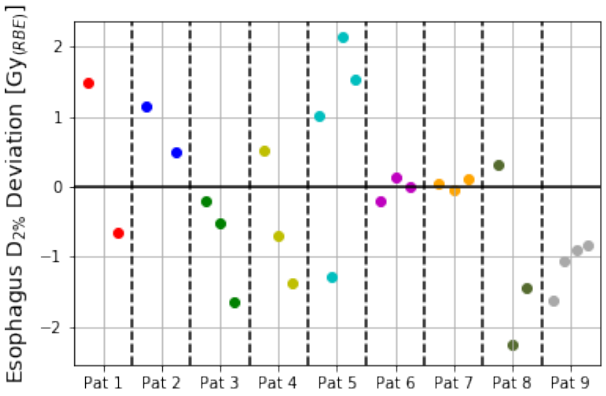

Figure 16: Esophagus $D_{2\%}$ deviation from the planning CT for respective verification CT.

Table 7: Esophagus $D_{2\%}$ determined from the planning CT for each patient.

planCT	Pat 1	Pat 2	Pat 3	Pat 4	Pat 5	Pat 6	Pat 7	Pat 8	Pat 9
Esophagus $D_{2\%}$ [$Gy_{(RBE)}$]	14.3	15.3	26.8	23.5	9.5	27.2	29.4	28.3	30.4

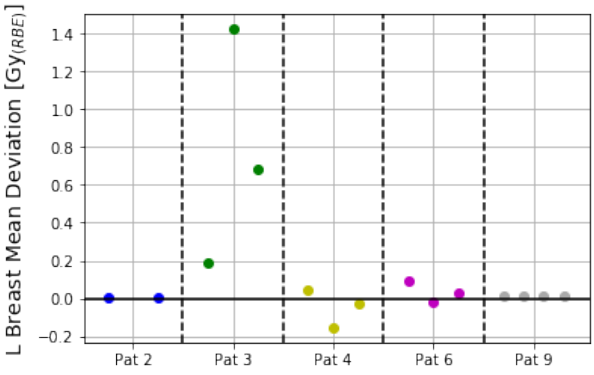

(a) L Breast D_{mean}

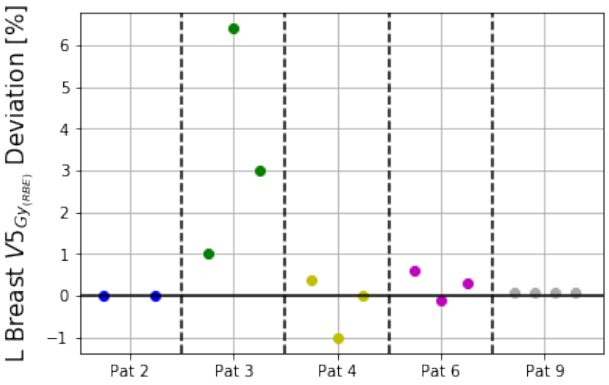

(b) L Breast $V_{5\text{Gy}_{(RBE)}}$

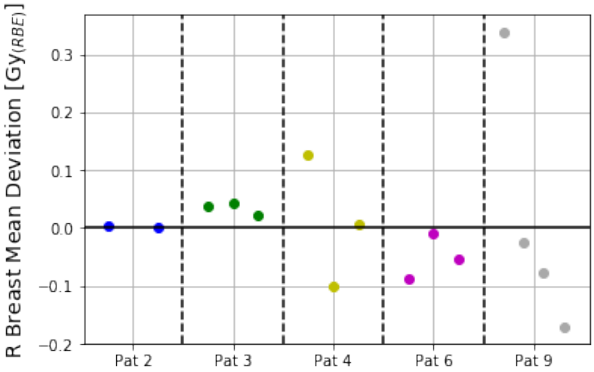

(c) R Breast D_{mean}

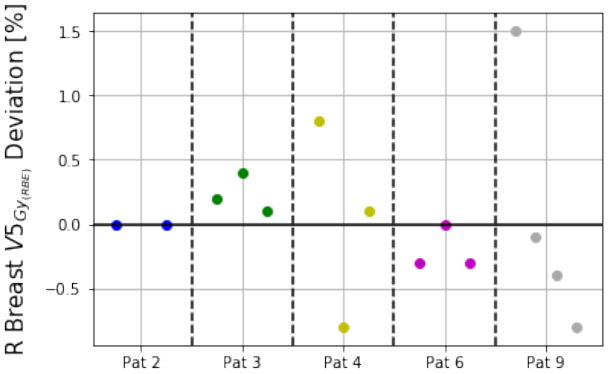

(d) R Breast $V_{5\text{Gy}_{(RBE)}}$

Figure 17: Left (a) and Right Breast (b) D_{mean} and absolute $V_{5\text{Gy}_{(RBE)}}$ deviation from the planning CT for respective verification CT.

Table 8: Left and Right Breast D_{mean} and $V_{5Gy_{(RBE)}}$ determined from planning CT for each patient.

planCT	Pat 2	Pat 3	Pat 4	Pat 6	Pat 9
L Breast D_{mean} [$Gy_{(RBE)}$]	0.0	7.4	1.0	0.3	0.0
L Breast $V_{5Gy_{(RBE)}}$ [%]	0.0	39.8	7.5	2.1	0.1
R Breast D_{mean} [$Gy_{(RBE)}$]	0.0	0.9	2.1	1.1	2.7
R Breast $V_{5Gy_{(RBE)}}$ [%]	0.0	6.1	16.0	7.6	13.1

4.3 Part 3: Treatment plans with smaller margins

The dosimetric analysis of the TPs with smaller margins, **P1 5mm 4.5**%, **P2 3mm 4.5**% and **P3 5mm 3.5**%, in comparison with the original plan, **P0 7mm 4.5**%, is presented for each patient in figure 18a-i, where CTV $D_{98\%}$ for the pCT (black points) and vCTs (colored points) is displayed. In addition, the robust evaluation with respect to CTV $D_{98\%}$ conducted for each new plan is also displayed in figure 18a-i, where each coloured point is a different uncertainty scenario.

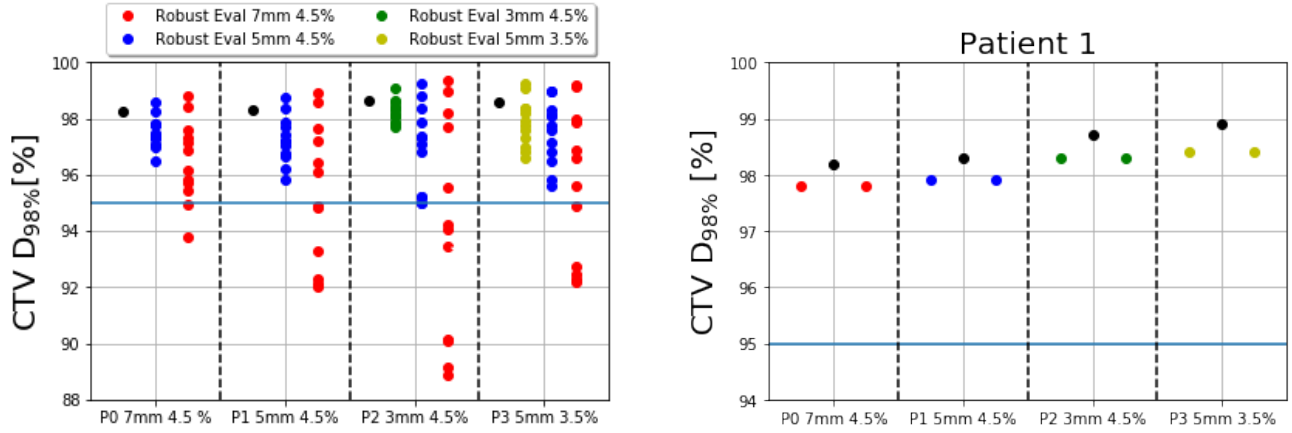

(a)

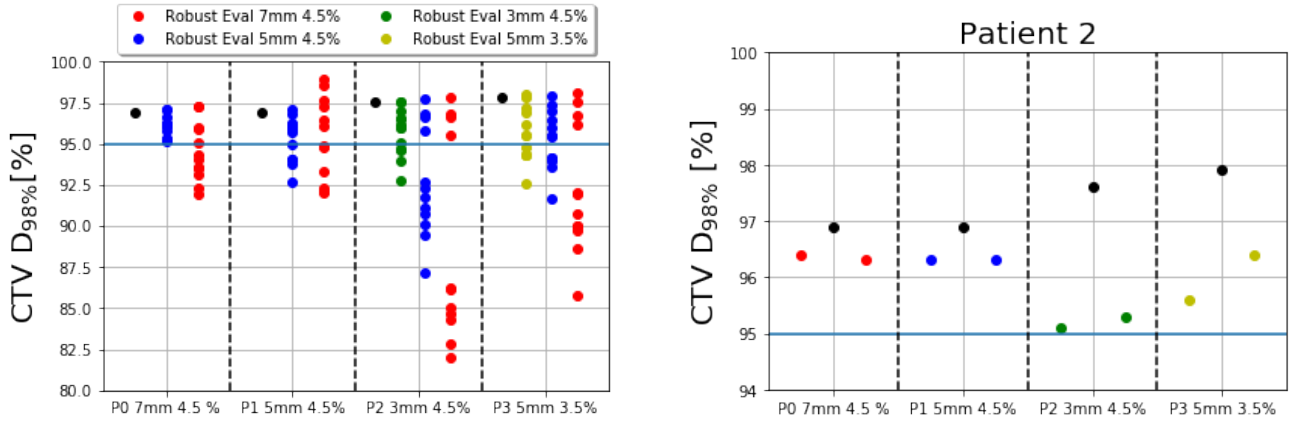

(b)

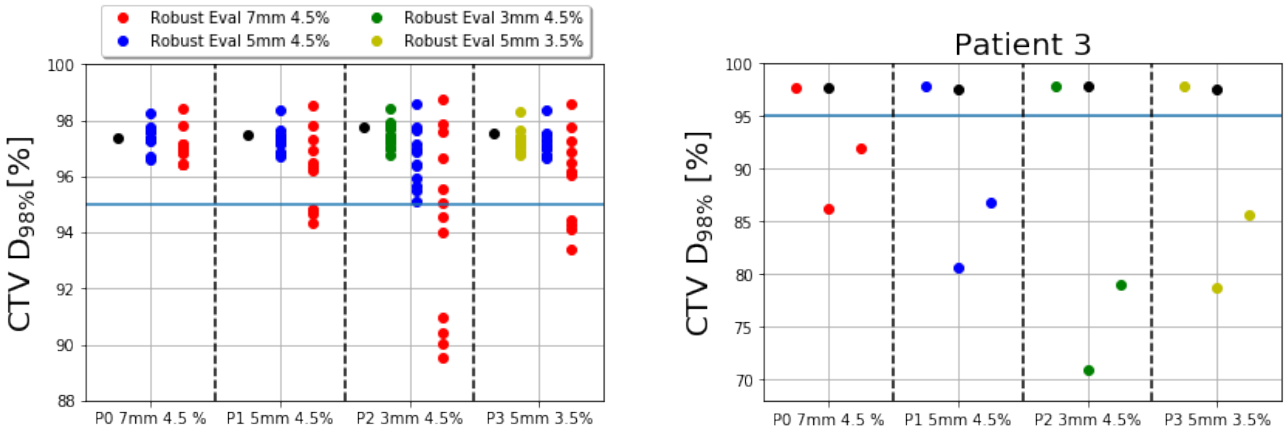
Robust Eval 7mm 4.5%
Robust Eval 5mm 4.5%
Robust Eval 3mm 4.5%
Robust Eval 5mm 3.5%
CTV D98%[%]
P0 7mm 4.5 %
P1 5mm 4.5%
P2 3mm 4.5%
P3 5mm 3.5%
Patient 3

(c)

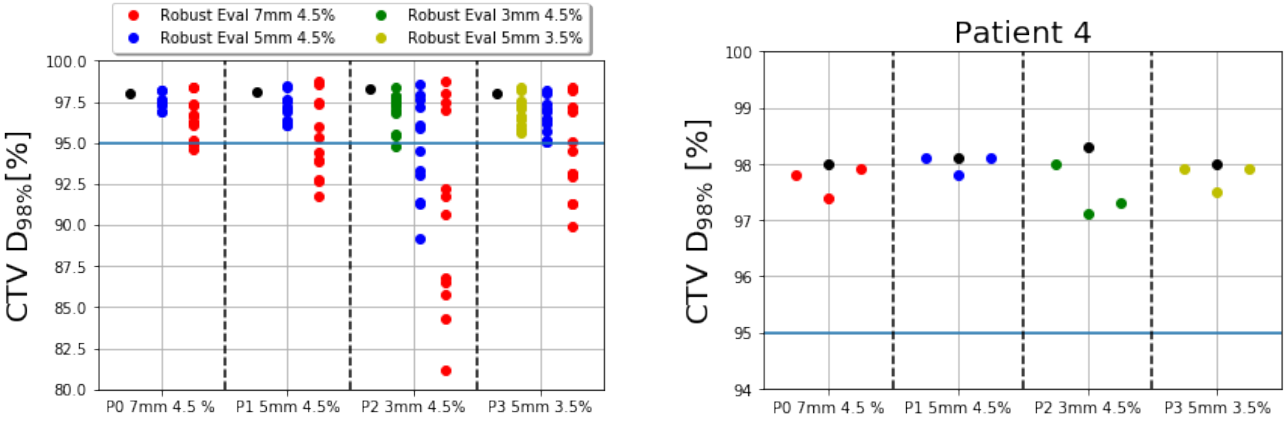
Robust Eval 7mm 4.5%
Robust Eval 5mm 4.5%
Robust Eval 3mm 4.5%
Robust Eval 5mm 3.5%
CTV D98%[%]
P0 7mm 4.5 %
P1 5mm 4.5%
P2 3mm 4.5%
P3 5mm 3.5%
Patient 4

(d)

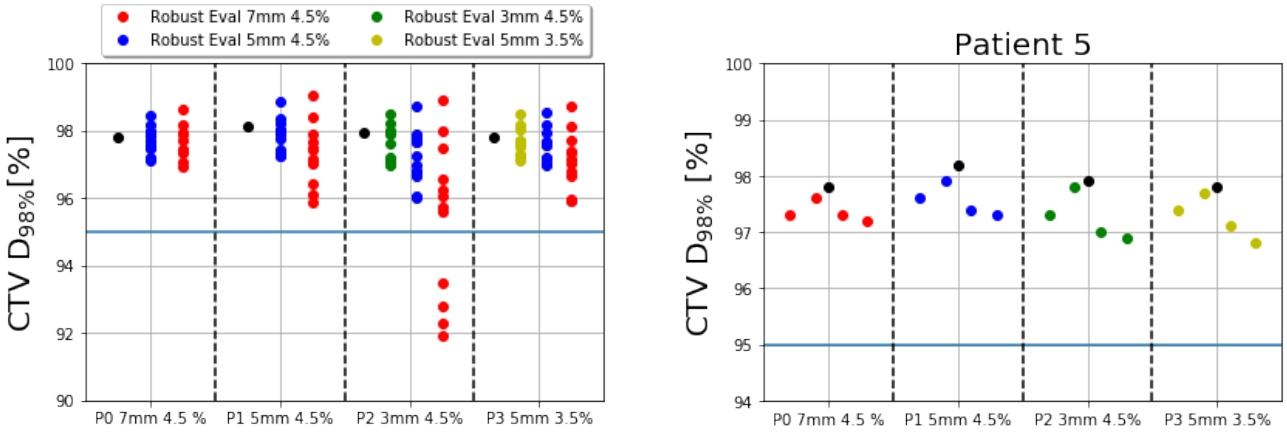
Robust Eval 7mm 4.5%
Robust Eval 5mm 4.5%
Robust Eval 3mm 4.5%
Robust Eval 5mm 3.5%
CTV D98%[%]
P0 7mm 4.5 %
P1 5mm 4.5%
P2 3mm 4.5%
P3 5mm 3.5%
Patient 5

(e)

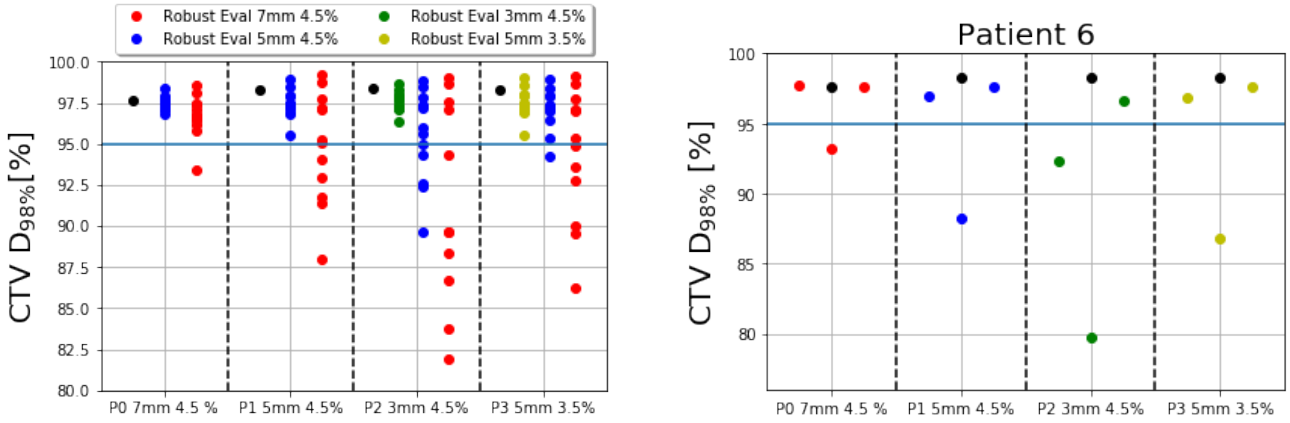
Robust Eval 7mm 4.5%
Robust Eval 5mm 4.5%
Robust Eval 3mm 4.5%
Robust Eval 5mm 3.5%
CTV D98%[%]
P0 7mm 4.5 %
P1 5mm 4.5%
P2 3mm 4.5%
P3 5mm 3.5%
Patient 6

(f)

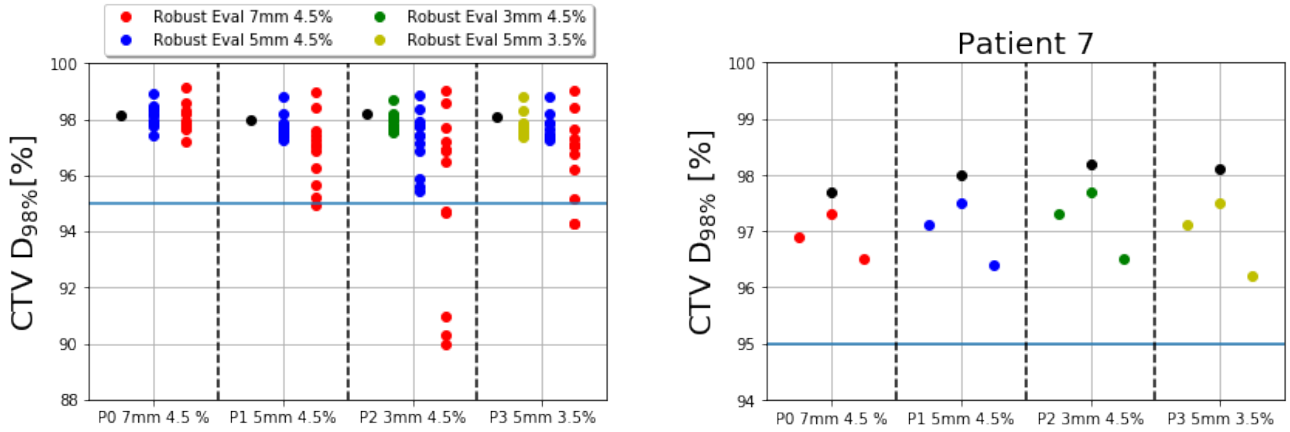
Robust Eval 7mm 4.5%
Robust Eval 5mm 4.5%
Robust Eval 3mm 4.5%
Robust Eval 5mm 3.5%
CTV D98%[%]
P0 7mm 4.5 %
P1 5mm 4.5%
P2 3mm 4.5%
P3 5mm 3.5%
Patient 7

(g)

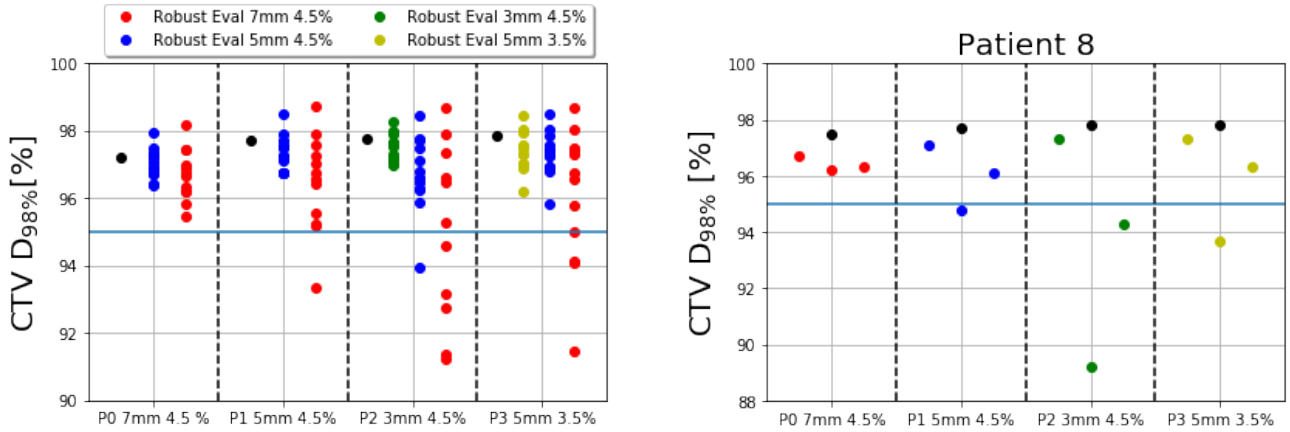
Robust Eval 7mm 4.5%
Robust Eval 5mm 4.5%
Robust Eval 3mm 4.5%
Robust Eval 5mm 3.5%
CTV D98%[%]
P0 7mm 4.5 %
P1 5mm 4.5%
P2 3mm 4.5%
P3 5mm 3.5%
Patient 8

(h)

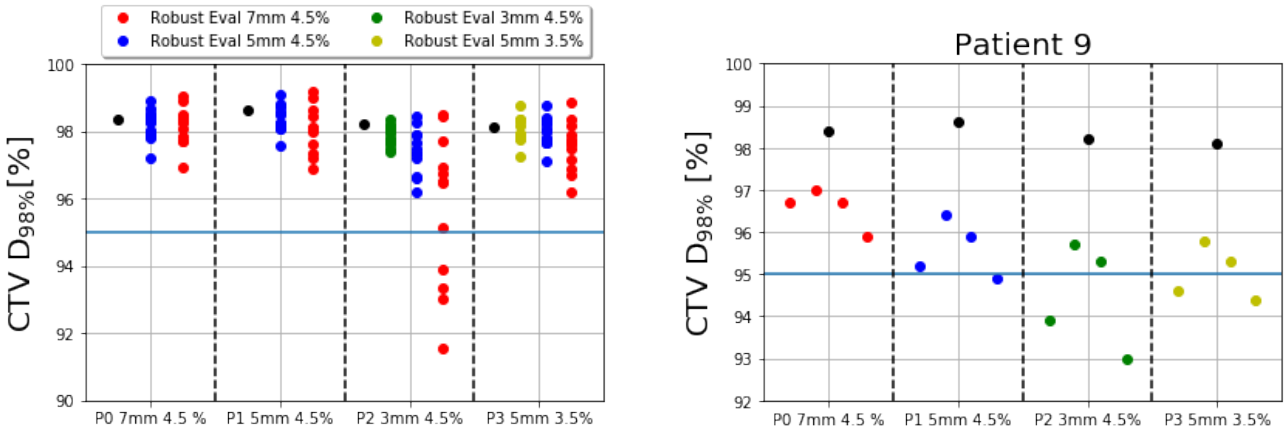

(i)

Figure 18: Treatment plans with smaller margins for each patient (a-i) with corresponding CTV $D_{98\%}$ and robust evaluation. The black dots represents the dose achieved at the pCT and the blue line represents dose criteria for CTV $D_{98\%}$, i.e. CTV $D_{98\%} \geq 95\%$. The colored points at the left figures represents CTV $D_{98\%}$ at the vCTs, where the first acquired vCT is the furthest to the left. The colored points at the robust evaluation is each a different uncertainty scenario with the resulting CTV $D_{98\%}$ achieved in that scenario.

The volume of the 95% isodose for all TPs normalized with $D_{95\%}$ isodose structure from the original plan is presented in figure 19.

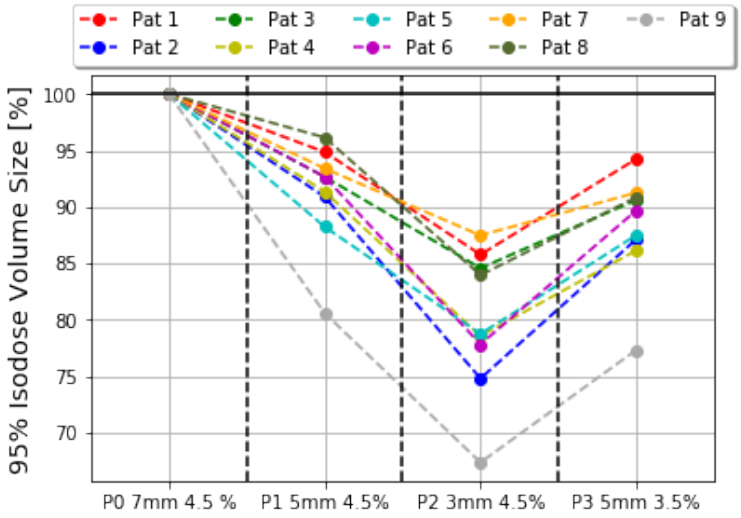

Figure 19: Relative volume of 95% isodose volume for all TPs, normalized with the volume of the 95% isodose structure from original plan.

For all TPs, the mean dose received by the heart and total lung volume and Heart $V15_{Gy}$ and LungTot $V5_{Gy}$ at the pCT is presented in table 9-10 for each patient. In addition, mean dose received by left and right breast for the female patients is displayed in table 11.

Table 9: Mean dose ($\overline{D}$) and dose volume metrics ($V15_{Gy_{(RBE)}}$, $V5_{Gy_{(RBE)}}$) received by heart and total lung volume from all plans on the pCT for the **male** patients.

Patient 1	$\overline{D}_{Heart}$ [$Gy_{(RBE)}$]	$\overline{D}_{LungTot}$ [$Gy_{(RBE)}$]	Heart $V_{15Gy_{(RBE)}}$ [%]	LungTot $V_{5Gy_{(RBE)}}$ [%]
P0 7mm 4.5%	0.90	0.74	1.4	4.4
P1 5mm 4.5%	0.80	0.63	1.3	4.0
P2 3mm 4.5%	0.68	0.55	1.1	3.5
P3 5mm 3.5%	0.81	0.63	1.3	4.0
Patient 5	$\overline{D}_{Heart}$ [$Gy_{(RBE)}$]	$\overline{D}_{LungTot}$ [$Gy_{(RBE)}$]	Heart $V_{15Gy_{(RBE)}}$ [%]	LungTot $V_{5Gy_{(RBE)}}$ [%]
P0 7mm 4.5%	4.96	3.20	13.8	14.4
P1 5mm 4.5%	4.48	2.86	12.2	13.1
P2 3mm 4.5%	3.89	2.54	10.6	11.7
P3 5mm 3.5%	4.35	2.80	11.8	12.8
Patient 7	$\overline{D}_{Heart}$ [$Gy_{(RBE)}$]	$\overline{D}_{LungTot}$ [$Gy_{(RBE)}$]	Heart $V_{15Gy_{(RBE)}}$ [%]	LungTot $V_{5Gy_{(RBE)}}$ [%]
P0 7mm 4.5%	3.11	3.30	9.0	15.9
P1 5mm 4.5%	2.93	3.05	8.5	14.8
P2 3mm 4.5%	2.68	2.81	7.9	13.6
P3 5mm 3.5%	2.86	3.00	8.3	14.5
Patient 8	$\overline{D}_{Heart}$ [$Gy_{(RBE)}$]	$\overline{D}_{LungTot}$ [$Gy_{(RBE)}$]	Heart $V_{15Gy_{(RBE)}}$ [%]	LungTot $V_{5Gy_{(RBE)}}$ [%]
P0 7mm 4.5%	6.22	3.36	18.9	17.2
P1 5mm 4.5%	5.95	3.11	18.3	15.9
P2 3mm 4.5%	5.22	2.68	16.0	14.0
P3 5mm 3.5%	5.74	3.00	17.6	15.5

Table 10: Mean dose ($\overline{D}$) and dose volume metrics ($V15_{Gy_{(RBE)}}$, $V5_{Gy_{(RBE)}}$) received by heart and total lung volume from all plans on the pCT for the **female** patients.

Patient 2	$\overline{D}_{Heart}$ [$Gy_{(RBE)}$]	$\overline{D}_{LungTot}$ [$Gy_{(RBE)}$]	Heart $V_{15Gy_{(RBE)}}$ [%]	LungTot $V_{5Gy_{(RBE)}}$ [%]
P0 7mm 4.5%	0.36	1.36	0.1	8.9
P1 5mm 4.5%	0.29	1.23	0	7.6
P2 3mm 4.5%	0.22	1.05	0	6.5
P3 5mm 3.5%	0.28	1.19	0	7.4
Patient 3	$\overline{D}_{Heart}$ [$Gy_{(RBE)}$]	$\overline{D}_{LungTot}$ [$Gy_{(RBE)}$]	Heart $V_{15Gy_{(RBE)}}$ [%]	LungTot $V_{5Gy_{(RBE)}}$ [%]
P0 7mm 4.5%	4.44	5.28	12.9	24.1
P1 5mm 4.5%	4.09	4.91	11.9	22.7
P2 3mm 4.5%	3.72	3.91	10.8	21.4
P3 5mm 3.5%	4.05	4.87	11.7	22.6
Patient 4	$\overline{D}_{Heart}$ [$Gy_{(RBE)}$]	$\overline{D}_{LungTot}$ [$Gy_{(RBE)}$]	Heart $V_{15Gy_{(RBE)}}$ [%]	LungTot $V_{5Gy_{(RBE)}}$ [%]
P0 7mm 4.5%	3.63	3.42	10.6	17.9
P1 5mm 4.5%	3.25	3.16	9.5	16.5
P2 3mm 4.5%	2.94	2.63	8.5	13.8
P3 5mm 3.5%	3.17	3.05	9.3	16.0
Patient 6	$\overline{D}_{Heart}$ [$Gy_{(RBE)}$]	$\overline{D}_{LungTot}$ [$Gy_{(RBE)}$]	Heart $V_{15Gy_{(RBE)}}$ [%]	LungTot $V_{5Gy_{(RBE)}}$ [%]
P0 7mm 4.5%	4.75	3.06	15.2	15.1
P1 5mm 4.5%	4.29	2.80	13.5	14.1
P2 3mm 4.5%	3.68	2.48	11.5	12.9
P3 5mm 3.5%	4.26	2.76	13.4	14.0
Patient 9	$\overline{D}_{Heart}$ [$Gy_{(RBE)}$]	$\overline{D}_{LungTot}$ [$Gy_{(RBE)}$]	Heart $V_{15Gy_{(RBE)}}$ [%]	LungTot $V_{5Gy_{(RBE)}}$ [%]
P0 7mm 4.5%	1.00	3.15	1.1	14.0
P1 5mm 4.5%	0.57	2.65	0.2	12.1
P2 3mm 4.5%	0.32	2.31	0	10.8
P3 5mm 3.5%	0.54	2.62	0.2	11.9

Table 11: Mean dose ($\overline{D}$) received by left and right breast from all plans on the pCT for the **female** patients.

Patient 2	$\overline{D}_{L-Breast}$ [Gy$_{(RBE)}$]	$\overline{D}_{R-Breast}$ [Gy$_{(RBE)}$]
P0 7mm 4.5%	0	0
P1 5mm 4.5%	0	0
P2 3mm 4.5%	0	0
P3 5mm 3.5%	0	0
Patient 3	$\overline{D}_{L-Breast}$ [Gy$_{(RBE)}$]	$\overline{D}_{R-Breast}$ [Gy$_{(RBE)}$]
P0 7mm 4.5%	6.47	1.09
P1 5mm 4.5%	5.93	1.02
P2 3mm 4.5%	5.51	1.03
P3 5mm 3.5%	5.89	1.01
Patient 4	$\overline{D}_{L-Breast}$ [Gy$_{(RBE)}$]	$\overline{D}_{R-Breast}$ [Gy$_{(RBE)}$]
P0 7mm 4.5%	1.10	2.32
P1 5mm 4.5%	1.01	2.16
P2 3mm 4.5%	0.84	1.84
P3 5mm 3.5%	0.99	2.13
Patient 6	$\overline{D}_{L-Breast}$ [Gy$_{(RBE)}$]	$\overline{D}_{R-Breast}$ [Gy$_{(RBE)}$]
P0 7mm 4.5%	0.31	1.19
P1 5mm 4.5%	0.29	1.08
P2 3mm 4.5%	0.25	1.00
P3 5mm 3.5%	0.29	1.08
Patient 9	$\overline{D}_{L-Breast}$ [Gy$_{(RBE)}$]	$\overline{D}_{R-Breast}$ [Gy$_{(RBE)}$]
P0 7mm 4.5%	0.03	2.71
P1 5mm 4.5%	0.02	2.28
P2 3mm 4.5%	0.01	1.88
P3 5mm 3.5%	0.02	2.20

5 Discussion

5.1 Evaluation of the Image Registration

Throughout treatment, dose-planning and dose-evaluation are based on contours delineated on various medical images. In order to ensure an effective treatment and adequate OAR sparing, these contours must to a high degree correctly represent the underlying, *true*, anatomy of the patient. However, the lack of quantitative validation in image registration and contour segmentation constitutes one of the key challenge in these types of studies. Volume based evaluation, such as DSC (see equation (3)), can be used but as mentioned in section 2.6.2 the DSC-measurement provides no information regarding the anatomical "point-to-point" correspondence precision from the registration. This is the reason why, similar to other studies[31][32][33], the accuracy of the generated DIR contours were evaluated solely based on visual inspection.

The qualitative evaluation of transferred contours performed in this thesis (see table 4) demonstrated that around 20% of rigid contours required major modifications (evaluated as "3") before being clinically acceptable, whereas no deformed contours required major modifications. Additionally, around 40% of rigid contours were evaluated as having minor deviations (graded as "2") from the underlying anatomical volume while the corresponding number for deformed contours was only 8%. This means that 40% of the rigid

contours and 92% of the deformed contours required no modifications (graded as "1"), demonstrating the accuracy of DIR-generated contours in correctly representing the underlying anatomical volumes. However, it should be clarified that for some patients, more rigid transferred contours graded "2" and "3" were seen than for others, noticeable patient 3, 5 and 6, highlighting that individual evaluation of each patient is important. These three patients all demonstrated large relative lung volume deviation from the pCT, seen in figure 11b, which is likely the reason why the rigid transferred contours required major modifications before being clinically acceptable. This is obvious when looking at figure 10 where the RIR could not handle the large displacement of the lungs but the DIR could. However, there are also other factors than large lung volume variation that affect the RIR as patient 6 only had large lung volume deviation at the second vCT but yielded bad rigid contours throughout treatment. Plausible factors are variation in the position of the diaphragm and heart or variation in body contour, which are parameters evaluated to assess the patients reproducibility of DIBH (see section 2.1.2), however, these were not evaluated in this thesis. Furthermore, only patient 3 and 6 provided deformed contours graded "2" or higher, whereas for the rest of the patients, including patient 5, only had contours graded as "1". Interestingly, for patient 5 the DIR algorithm within Eclipse^{TM} was able to accurately deform contours despite the large relative lung volume deviation. Patient 7-9 had not been included in the study before evaluating the accuracy of the DIR and RIR algorithm within Eclipse^{TM}. As such, it was assumed that the deformed transferred contours for these patients followed the same trend as for patient 1-6, i.e. that *all* included deformed contours would be clinical acceptable.

One important note concerning the IR evaluation is that only one physician evaluated the contours. However, there exists an inter-variation between observers when delineating/evaluating contours, which arise from disagreement between physicians/radiation oncologists on target extension as well as from misinterpretation/lack of delineation protocols[35]. This variation/error in delineation persists throughout the course of RT-treatment, and as a result has a large impact on the resulting dose to the tumor. Consequently, due to this inherent bias in delineation/evaluating more physicians would need to be incorporated in this study before implementing the findings within the clinical work.

5.1.1 Similar studies of Image Registration Evaluation

In a similar study, Vickress et al[19] evaluated the accuracy of Varian's Eclipse^{TM} in radiation therapy for patients with lesions in the thoracic region. Contours investigated included GTV, heart, esophagus and left and right lungs, similar to this thesis. They compared the propagation accuracy of deformed and rigid contours with human-made ones by constructing the DSC value between each contour. Results were evaluated in accordance with guidelines given by AAPM TG 132 (American Association of Physicists in Medicine: Task Group 132), which states that DSC larger than 0.8-0.9 is an indication of a relatively good agreement. The results showed that the DSC coefficient was on average above 0.9 for the heart and lung structure, which fulfills the TG-132 criteria. On the other hand the esophagus received an average DSC of 0.61, however, the authors concluded, this was a consequence of the relative high surface area of the esophagus but also inter-variations among observers in delineating the esophagus. GTV received an average DSC value of 0.72 which Vickress et al also determined to partially be explained by large inter-observer variability in delineation. However, all deformed contours produced higher DSC values than their rigid counterparts, an indication that deformed contours better represent the underlying anatomical volume which is in agreement

with the conclusion from our qualitative study performed in this thesis.

Additionally, a study by Ramadaan et al[36] concluded that Varian's DIR (Eclipse^{TM}) for the head and neck area provided structures which in 92% of the cases required no or only minor modifications based on a similar grading curve as in this thesis. They also conducted a quantitative analysis by computing DSC between DIR structures and DIR structures modified by a radiation oncologist which showed an average DSC of 93%. However, considerably smaller volumetric overlap was observed between independently re-contoured contours, i.e. new delineation of contours on vCTs, and DIR generated ones, which on average was 82%. The conclusion was that there exists a potential bias towards approving DIR structures when directly evaluating how accurately they represent the anatomic volume. A similar potential bias therefore exists within the qualitative evaluation conducted in this thesis as well since the physician who performed the evaluation was only asked to validate *already* deformed contours.

5.2 Evaluation of the original treatment plan

From both the geometric and dosimetric analysis of the original plan throughout treatment (see figure 11-17) it is understood that the pCT only captures a snapshot of the patient's anatomy, which due to uncertainties, e.g. set-up, range, reproducibility of DIBH or other changes, e.g. weight gain/loss, will not be a perfect representation of the patient throughout treatment. This has the potential to create a sub-optimal dose distributions during treatment with unforeseen consequences, e.g. under-dosing CTV or over-dosing OARs.

5.2.1 Volume variations and dose-deviations

Variations in CTV and total lung volume (see figure 11) throughout treatment were seen for all patients, with a relative volume deviation up to $\pm 10\%$ and $\pm 25\%$ for the CTV and the total lung volume, respectively, for some patients. Interestingly, patient 7 and 8 experienced the biggest changes in total lung volume (figure 11) but had a robust dose to CTV throughout treatment with their original plan (figure 13), i.e. the prescribed dose was delivered to CTV despite potential uncertainties. This suggests that total lung volume deviation alone does not predict the robustness for CTV. Patient 3 and 6 on the other hand, whom both also experienced large total lung volume deviation, did not achieve CTV $D_{98\%} \geq 95\%$ throughout treatment with their original plan (7 mm/ 4.5%). For patient 3, the reproducibility of DIBH was significantly different and CTV $D_{98\%}$ as low as 86% and replanning was therefore performed. All other patients had a robust dose to CTV throughout treatment (see figure 13). Some of the patients, noticeable patient 1, 4 and 5, had a much higher robustness than the others, a clear indication that smaller margins could be possible and still ensure a robust dose to CTV.

The dose to OARs did as well differ from that received on the pCT, another example that the pCT is only a snapshot of the patient's anatomy which will differ throughout treatment. However, for most patients these dose deviations for the OARs were minuscule. The maximum change in mean dose to LungTot was 0.6 Gy for patient 6 and 9 (lower dose) and 0.5 Gy for patient 5 (higher dose), while $V5_{Gy}$ and $V15_{Gy}$ changed only at maximum 3%. For the female patients variations in mean dose to the left and right breasts were also minuscule with mean dose to the right breast having a maximum deviation of 0.3 Gy. For patient 3 mean dose to the left breast increased by 1.4 Gy, most likely due to the patients' poor reproducibility.

All other female patients experienced only a ± 0.2 Gy variation throughout treatment. The OAR with by far the largest deviations was the heart. For most patients the maximum heart mean dose deviation was restricted to ± 1 Gy, however for patient 3, 6, and 8, heart mean dose deviations of up to 5 Gy were seen. All these patients demonstrated a large relative total lung volume deviation, most likely placing the heart in an unfavorable position, suggesting total lung volume variations as a possible geometrical indicator for dosimetric variations. On the other hand patient 6 only had large total lung volume deviation at her second vCT, with almost no volume deviation at her other vCTs, despite that a higher mean dose to the heart of around 1.5 Gy was observed at these vCTs as well. Other possible geometrical changes could be baseline and breath-hold amplitude, position of diaphragm or small in-homogeneity located in the beam path, however these were not evaluated in this thesis.

A study by Andersson et al[12] assessed inter breath-hold variations between CT images, pCT and vCTs, by quantifying well-defined distances in the thorax region. In one sagittal image-slice, the distance between the vertebra and sternum were computed at two locations. Additionally, in the axial slices well-defined distances were determined. Illustration of these distances are presented in Appendix A. Geometric measurements similar to these could potentially be used to quantify the acceptable limits of a patients DIBH reproducibility before too large dose-deviations are observed. Any geometric measurement which could predict dosimetric-deviations during treatment would be desired such that it can be incorporated within the TP-optimizing.

In summary, when comparing geometric with dosimetric evaluations, it is understood that these are related but not equivalent, which has previously been shown by other studies[34].

5.2.2 Hausdorff distances

Figure 13 is a strong indicator that smaller margins than 7 mm and 4.5% are possible for most patients as long as the patients reproducibility is within certain limits. In this thesis the Hausdorff distance formalism was used to establish an overview of the extent of set-up margin required for each planning CTV in order to cover each deformed CTV contour throughout treatment. Note that only patient 1-6 were incorporated in this part of the geometrical analysis. The extent of displacement, see figure 12, within all orientations was determined to be between 1-7 mm with the most and highest displacement seen mostly for patient 3 and 6 which agrees with the findings of the dosimetric analysis. For all other patients a 5 mm or even 3 mm, symmetric expansion of the planning CTV would be sufficient throughout treatment. However, as mentioned in section 2.6.2 each deformed CTV had to be propagated back to the pCT with a RIR. As these HD calculations is of mm scale incorrect voxel-mapping or some small displacement within the RIR could shift the deformed CTVs resulting in incorrect HD values. Perfect alignment between the images is not possible, consequently, it is the accuracy of the RIR algorithm which determines the uncertainty for these HD calculations. Conclusively it was determined that the geometrical analysis with the HD formalism is *not* a definitive demonstration of set-up uncertainties, only an intuitive validation that set-up margins used today is sufficient in covering CTV throughout treatment. One could argue that patient 3 and 6 were within 7 mm displacement but still demonstrated low robustness to CTV. This highlights once again that geometric and dosimetric evaluations are related but not equivalent and the degree at which a geometric variation will have on the resulting dose distribution is a complex problem within proton therapy.

Highest HD displacement were seen in the SI orientation which inevitably describes motion in the two other orientations, AP and LR, i.e. the HD calculations within one orientation describes motion in the other two. As three orientations were evaluated information about displacement for each orientation is given two times and one excepts that the HD calculations for a given orientation is the same regardless of which orientation is was determined within, i.e. the Anterior-Posterior- displacement is the same in the Left-Right orientation as in the Superior-Inferior one. This was not the case, clearly understood from figure 12. A plausible reason for this is the difference in resolution between the orientations as the number of pixels in the SI orientation were 512x512 while the pixels in the other orientations were only 192-214 times 512.

In summary, figure 13, displaying CTV $D_{98\%}$ acquired at the vCTs, is the strongest indicator that smaller margins in the RO-process could be possible, while the geometric evaluation of HD distances seen in figure 12 demonstrates that for most patients a 5 mm symmetric expansion of the planning CTV would be sufficient as set-up uncertainty margin.

5.3 Treatment plans with smaller margins

5.3.1 Robustness to CTV of treatment plans with smaller perturbations

In all cases utilizing smaller perturbations in the RO-process generates TPs with similar CTV $D_{98\%}$ variation or worse than in the original plan throughout treatment, understood from figure 18, with an increasing variation when using smaller margins. The only exception was seen for patient 4s treatment plan P1 5 mm 4.5% where a smaller CTV $D_{98\%}$ variation than in the original plan was observed (figure 18b), which was concluded to be a consequence of the inverse/iterative dose-planning process. With inverse/iterative dose-planning, the same starting conditions can result in slight variations in the optimized TP. TPs with smaller perturbations are still required to deliver a robust dose to CTV and despite dose-criteria of CTV $D_{98\%} \geq 95\%$ it is not desirable if a resulting dose-distribution scarcely achieves this, i.e. $D_{98\%} \geq 95\%$ should not only barely be achieved. With this in mind one can conclude that at least for five out of the nine patients, TPs with a symmetric 5 mm and 4.5%/3.5% range-uncertainty would suffice in delivering a robust dose to CTV, demonstrating that smaller margins are possible. Even P2 3mm 4.5% would suffice for four out of the patients. Patient 8 and 9 only scarcely achieved a robust dose to CTV throughout treatment with plan P1 5mm 4.5% whereas P2 and P3 would under-dose the CTV. Hence, utilizing 3.5% range-uncertainty instead of 4.5% generate in most cases a less robust TP, increasing the risk for under-dosing CTV (figure 18). In addition, the difference between the high dose volume size (95% isodose volume size, figure 19) of TPs optimized with 5 mm/3.5% and 5mm/4.5% were minuscule, being at maximum 5% less for P3 than P1. Thus, no great variation in OAR doses were observed (table 10-11), suggesting that not much is gained in reducing the range-uncertainty from 4.5% to 3.5% with respect to the increased risk of under-dosing CTV (i.e. less robust TP).

Most patients had a robust dose to CTV with their original plan which was not the case for patient 3 and 6. Regardless of the insufficient target coverage with their original TPs, TPs with smaller margins were created for these as well with the same settings and criteria as the original plan (see section 3.4.1). As expected, utilizing smaller margins results in an even worse target coverage than in the original plan.

In the worst case CTV $D_{98\%}$ dropped from 86% to 70% for patient 3 and from 93% to 80% for patient 6, demonstrating that an already critical plan becomes more critical when using smaller margins. The poor reproducibility for these patients (patient 3 throughout treatment, patient 6 only at her second vCT) is most likely the reason for the large CTV $D_{98\%}$ variation, consequently if implementing smaller margins, knowledge about the DIBH reproducibility at an early stage such that under-dosing CTV can be prevented is required. The patients ability to reproduce the same DIBH at every fraction is evaluated at the home clinic, however, it is most likely impossible to predict which patients will suddenly have poor reproducibility during their treatment. The DIBH reproducibility evaluation could potentially be more accurate if more DIBH-evaluating CT images are acquired (currently two additional CT images and the pCT is used), however, this would increase the workload at the home clinic. Likewise, replanning, as discussed in section 2.2, would be required to a greater extent for patients who demonstrate poor DIBH reproducibility, increasing the workload further, both at the home clinic and at the Skandion clinic.

5.3.2 Robust evaluation of treatment plans with smaller perturbations

It was hypothesized that when using smaller margins in the optimization process one essentially creates a plan less robust than treatment plans with larger margins. As such all new treatment plans were robust evaluated with the same uncertainty parameters as used in the creation of respective BSPTV as well as with a symmetric 5 and 7 mm geometric displacement and a 4.5% range-uncertainty. From figure 18, it is clear that optimizing with smaller margins generates a less robust plan, i.e. less robust against possible uncertainties, than TPs optimized with larger margins. Essentially, by lowering the margin requirement higher demands for the patients reproducibility and more confidence in correct patient positioning, beam delivery, correct conversion from HU values into stopping power etc, are made. Additionally, robust evaluating all TPs with the same uncertainty parameters verifies that lowering the perturbations in the optimizer actually generates a less robust TP, i.e. the robustness of a TP is reflected by the perturbations used. Figure 19 also demonstrates this feature as smaller perturbations results in a smaller 95% isodose volume size. Lastly, the robust evaluation is not accurate if the patients reproducibility cannot be within certain limits, as patients with favorable robust evaluation, noticeable patient 3 (figure 18c), still had poor target coverage throughout treatment. In addition patient 2 (figure 18b) had poor robust evaluation but due to her ability to reproduce her DIBH this did not manifest throughout her treatment.

5.3.3 Reduction of high dose volume size

Another consequence of utilizing smaller margins around CTV/ITV is that the high dose volume, in this thesis evaluated by constructing the volume of the 95% isodose, becomes smaller (figure 19). This results in lower dose to all OARs, sparing them further than in the original plans. As expected, for all TPs with smaller margins the dose to normal tissue and OARs (table 9-10), is minimized. Mean Dose to the heart, lungs and left and right breast was lowered by 0.1 - 1 Gy, potentially reducing radiation-therapy associated side-effects. However, it should be clarified that the greatest benefits with smaller margins were seen for patients who with their original TP received large OAR doses ($>$ 1 Gy (RBE)). The CTV location for these patients was most likely in close proximity to these OARs which explain the large doses, as well as the high dose reduction with smaller margins. The other patients, where only a 0.1-0.3 Gy reduction in OAR doses were observed, might not benefit of an increased risk of under-dosing CTV. Consequently, smaller margins

are a trade-off between good target coverage and OAR sparing, as smaller margins are less robust but lowers the dose to OAR and normal tissue. Furthermore, the smaller 95% isodose-volume also means that the variation in dose received by OAR during treatment cannot be greater than that observed in the original plan (where bigger margins were used). This is the reason why an additional evaluation for dose variation of OARs at the vCTs throughout treatment for smaller margins was not conducted.

5.3.4 Robustness to CTV due to lung volume variations

For all but one patient where a low robustness with respect to CTV $D_{98\%}$ was observed, either in their original plan or TPs with smaller margins, also demonstrated a high relative lung total volume variation. The only exception was patient 9, who had a MFO plan in contrast to the other patients where SFUD plans were used. However, the implication that high relative lung total volume variation is the definite cause for low robustness to CTV with SFUD TPs is not true as both patient 5 and 7 also experienced large total lung volume variation but high robustness, i.e. at least for SFUD TPs low robustness to CTV implies large total lung volume variation but not the other way around. One plausible explanation could be that some CTV locations are more sensitive to lung variation than others. Only patients with CTV in the anterior thorax region were included in this study, which inevitably still constitute a large volume for possible CTV locations, e.g. CTV-expansions superior to the chest will most likely be less sensitive to lung volume variation than CTV-expansion inferior and left or right of sternum. As for patient 9 who had low robustness to CTV $D_{98\%}$ with smaller margins despite small relative total lung variations could be due to the lower robustness coherent with a MFO TP, previously discussed in section 2.4.2.1, and more MFO TPs would need to be evaluated in order to validate if the lower robustness seen for patient 9 is a consequence of the optimization technique used or some other factor(s).

6 Future prospects

It was concluded that at least for five out of the nine patients TPs a symmetric 5 mm and 4.5%/3.5% range-uncertainty would be sufficient in delivering a robust dose to CTV, demonstrating that smaller margins are possible. Within this work, patients with both good and bad reproducibility, as well as somewhere in between has been evaluated. However, in the interest of implementing the findings of this study in clinical RT more patients should be evaluated to establish an overview of the reproducibility seen in daily RT. Most interestingly when the degree of reproducibility directly affects the robustness to CTV, with for example if some CTV locations in the anterior thorax region are more sensitive to lung variation than others and in such case identifying which these are. This could be used as a prediction at an early stage about the potential risk with under-dosing CTV if the patient has poor DIBH reproducibility. It would also be interesting to include more CTV locations in close proximity of OARs, as it was for these patients where the most benefits of smaller margins were observed. The patients ability to reproduce their DIBH at every dose-delivering is also an important factor in ensuring a robust dose to CTV. Additionally, the extent of replanning required if implementing smaller margins could also be further investigated.

Furthermore, only one patient with a MFO TP was included in this study due to the limited available data. Due to the coherent lower robustness of MFO TPs it is possible that perturbations0 with smaller

margins than 7 mm is insufficient in ensuring a robust dose to the target volume. Henceforth, more MFO TPs would need to be evaluated before any assumption can be made. Lastly, the only changes from the original TPs with the new ones were the margins used RO-process with some exceptions of weights used in the optimization process, e.g. constraints on 105% isodose volume. As it was observed that smaller margins are possible, other settings previously left unchanged such as the spot spacing could be evaluated further to investigate the effect these settings might have on the robustness to CTV when used with smaller margins. Lastly, this study is based on the Eclipse^{TM} system and the functions available within. However, there are other treatment-planning systems, e.g. RayStation (Raysearch Laboratories, Stockholm, Sweden), where the findings from this study should be verified with.

7 Conclusion

The purpose of this thesis was to optimize treatment margins for HL PT treatment delivered in DIBH such that a robust dose is delivered to the target volume while simultaneously minimizing the dose received by normal tissue and OARs. Currently, a symmetric 7 mm displacement and 4.5% range-uncertainty is applied in the RO-process for HL patients. However, it was concluded in this study that for five of the nine patients, TPs with smaller margins in the RO-process, in particular a symmetric 5 mm displacement and 4.5% range-uncertainty, demonstrated favorable qualities with a sufficient robustness to CTV and lower dose to OARs. These properties might reduce treatment associated side-effects, which has been the major goal of modern research in treatment of HL. On the other hand, with smaller margins in the RO-process the risk for under-dosing CTV increases as the TP is less robust than TPs with larger margins. Ideally, if implementing smaller margins, knowledge about the DIBH reproducibility at an early stage such that under-dosing CTV can be prevented is required. Likewise, replanning would be required to a greater extent for patients who demonstrate poor DIBH reproducibility.

References

[1] Hodgkin's lymfom: Symptom och behandling, <www.Cancerfonden.se>, Accessed 2021-09-17

[2] Hodgkins lymfom: Nationellt vårdprogram, Version 3.0, (2020-12-08), <www.Cancercentrum.se>

[3] Daniel Molin, "Clinical investigation of PBS proton treatment in Hodgkin lymphoma patients", "PRO-Hodgkin", Version 2.0, (2019-10-28), <www.Cancercentrum.se>

[4] Anneli Edvardsson, Malin Kügele, Sara Alkner, Marika Enmark, Joakim Nilsson, Ingrid Kristensen, Elisabeth Kjellén, Silke Engelholm & Sofie Ceberg. (2019), "Comparative treatment planning study for mediastinal Hodgkin's lymphoma: Impact on normal tissue dose using deep inspiration breath hold proton and photon therapy", Acta Oncologica, 58:1, 95-104

[5] Dabaja, B. S., Hoppe, B. S., Plastaras, J. P., Newhauser, W., Rosolova, K., Flampouri, S., Mohan, R., Mikhaeel, N. G., Kirova, Y., Specht, L., & Yahalom, J. (2018). "Proton therapy for adults with mediastinal lymphomas: The International Lymphoma Radiation Oncology Group guidelines". Blood, 132(16), 1635-1646.

[6] Chang JY, Zhang X, Knopf A, Li H, Mori S, Dong L, Lu HM, Liu W, Badiyan SN, Both S, Meijers A, Lin L, Flampouri S, Li Z, Umegaki K, Simone CB 2nd, Zhu XR. (2017) "Consensus Guidelines for Implementing Pencil-Beam Scanning Proton Therapy for Thoracic Malignancies on Behalf of the PTCOG Thoracic and Lymphoma Subcommittee". Int J Radiat Oncol Biol Phys, 99(1):41-50.

[7] VO Hematologi, Onkologi och Strålningsfysik, Skånes Universitetssjukhus. "Strålbehandling av tumörer i mediastinum och/eller fossa supraclav", (English title: Radiation therapy of tumors in the mediastinum and/or fossa supraclav), Version 2.0. (2021-02-18).

[8] INTERNATIONAL ATOMIC ENERGY AGENCY (IAEA). Vienna, (2005). "Radiation Oncology Physics".

[9] Mohan, R., & Grosshans, D. (2017). "Proton therapy - Present and future". Advanced drug delivery reviews, 109, 26-44.

[10] Weber, D. C., Lim, P. S., Tran, S., Walser, M., Bolsi, A., Kliebsch, U., Beer, J., Bachtiary, B., Lomax, T., & Pica, A. (2020). "Proton therapy for brain tumours in the area of evidence-based medicine". The British journal of radiology, 93(1107).

[11] Jette D, Chen W.(2011) "Creating a spread-out Bragg peak in proton beams". Phys Med Biol, 56(11).

[12] Andersson KM, Edvardsson A, Hall A, Enmark M, Kristensen I, (2019) "Pencil beam scanning proton therapy of Hodgkin's lymphoma in deep inspiration breath-hold: A case series report". Tech Innov Patient Support Radiat Oncol. 2019 Dec:6-10.

[13] Schätti A, Zakova M, Meer D & Lomax A J. (2014) "The effectiveness of combined gating and re-scanning for treating mobile targets with proton spot scanning. An experimental and simulation-based investigation", Phys. Med. Biol. 59 3813.

[14] Marika Enmark, Jörgen Olofsson, Sofie Ceberg, Joakim Jonsson. (2018). "The impact on pencil beam scanning (PBS) proton therapy for mediastinal lymphoma from deep inspiration breath-hold (DIBH) variability". Physica Medica, Volume 52, Supplement 1, 2018, Page 159.

[15] "Riktlinjer för andningsanpassad protonstrålbehandling av Hodgkin lymfom". English title: Guidelines for implementing DIBH-PBS from a national working group within the Skandion framework. (2018). Available from Skandion quality system RMT+.

[16] INTERNATIONAL ATOMIC ENERGY AGENCY (IAEA), (2008). "RELATIVE BIOLOGICAL EFFECTIVENESS IN ION BEAM THERAPY. TECHNICAL REPORTS SERIES No. 461".

[17] Eric.J Hall and Amato J Giaccia, "Radiobiology for the radiologist", Lippincott Williams & Wilkins, 7:th edition, 2012

[18] International Commission on Radiation Units and Measurements. (2007). "ICRU Report 78: Prescribing, Recording, and Reporting Proton Beam Therapy".

[19] Vickress J, Rangel Baltazar MA, Afsharpour H. (2021). "Evaluation of Varian's SmartAdapt for clinical use in radiation therapy for patients with thoracic lesions". J Appl Clin Med Phys. 2021 Mar;22(3):150-156.

[20] International Commission on Radiation Units and Measurements. (2009). "ICRU Prescribing, Recording and Reporting Photon Beam Therapy. International Commissions on Radiation Units and Measurements: Report 62", Bethesda, MD, USA.

[21] International Commission on Radiation Units and Measurements. (1978). "ICRU Prescribing, Recording and Reporting Photon Beam Therapy. International Commissions on Radiation Units and Measurements: Report 50", Bethesda, MD, USA.

[22] Unkelbach J, Alber M, Bangert M, Bokrantz R, Chan TCY, Deasy JO, Fredriksson A, Gorissen BL, van Herk M, Liu W, Mahmoudzadeh H, Nohadani O, Siebers JV, Witte M, Xu H. (2018). "Robust radiotherapy planning". Phys Med Biol. 63(22):22TR02.

[23] Liu W, Zhang X, Li Y, Mohan R. (2012). "Robust optimization of intensity modulated proton therapy". Med Phys. 9(2):1079-91.

[24] Paganetti H.(2012). "Range uncertainties in proton therapy and the role of Monte Carlo simulations". Phys Med Biol. Jun 7;57(11)

[25] Sahoo N, Poenisch F, Zhang X, Li Y, Lii M, Li H, Gautam AS, Wu R, Gillin M, Zhu XR. (2018). "3D treatment planning system-Varian Eclipse for proton therapy planning". Med Dosim. 43(2):184-194.

[26] Bokrantz R, Fredriksson A. (2017). "Scenario-based radiation therapy margins for patient setup, organ motion, and particle range uncertainty". Phys Med Biol. 62(4):1342-1357..

[27] Yeung, D., McKenzie, C. and Indelicato, D.J. (2014), "A dosimetric comparison of intensity-modulated proton therapy optimization techniques for pediatric craniopharyngiomas: A clinical case study". Pediatr Blood Cancer, 61:89-94

[28] Oh, S., & Kim, S. (2017). Deformable image registration in radiation therapy. Radiation oncology journal, 35(2), 101-111.

[29] Taha AA, Hanbury A. (2015). "An efficient algorithm for calculating the exact Hausdorff distance". IEEE Trans Pattern Anal Mach Intell. Nov;37(11):2153-63.

[30] Zeng C, Plastaras JP, Tochner ZA, White BM, Hill-Kayser CE, Hahn SM, Both S. (2015). "Proton pencil beam scanning for mediastinal lymphoma: the impact of interplay between target motion and beam scanning". Phys Med Biol. Apr 7;60(7):3013-29.

[31] Guerrero T, Zhang G, Huang TC, Lin KP. (2004) "Intrathoracic tumour motion estimation from CT imaging using the 3D optical flow method". Phys Med Biol. Sep 7;49(17):4147-61.

[32] Mattes D, Haynor DR, Vesselle H, Lewellen TK, Eubank W. (2001). "Non-rigid multi-modality image registration". In: Sonka Milan, Hanson Kenneth M, Proc. SPIE 4322 (eds.). Medical Imaging 2001: Image Processing. San Diego, CA.

[33] Liu DC, Nocedal J. (1989). "On the limited memory BFGS method for large scale optimization. Math Program. 45(1-3):503-528.

[34] Wu Q, Ivaldi G, Liang J, Lockman D, Yan D, Martinez A. (2006)."Geometric and dosimetric evaluations of an online image-guidance strategy for 3D-CRT of prostate cancer". Int J Radiat Oncol Biol Phys. Apr 1;64(5):1596-609.

[35] Njeh C. F. (2008). "Tumor delineation: The weakest link in the search for accuracy in radiotherapy. Journal of medical physics", 33(4): 136-140.

[36] Ramadaan IS, Peick K, Hamilton DA, Evans J, Iupati D, Nicholson A, Greig L, Louwe RJ. (2015). "Validation of Varian's SmartAdapt deformable image registration algorithm for clinical application". Radiat Oncol. Mar 31;10:73.

Appendices

A Geometric measurements for inter breath-hold variations

Displayed in figure 20 are examples of well-defined distances in the thorax region which can be used to assess inter breath-hold variations between CT images, pCT and vCTs. Distance A and B describes the distance between the vertebra and sternum in the sagittal orientation, while distance C a well-defined distance in the axial orientation.

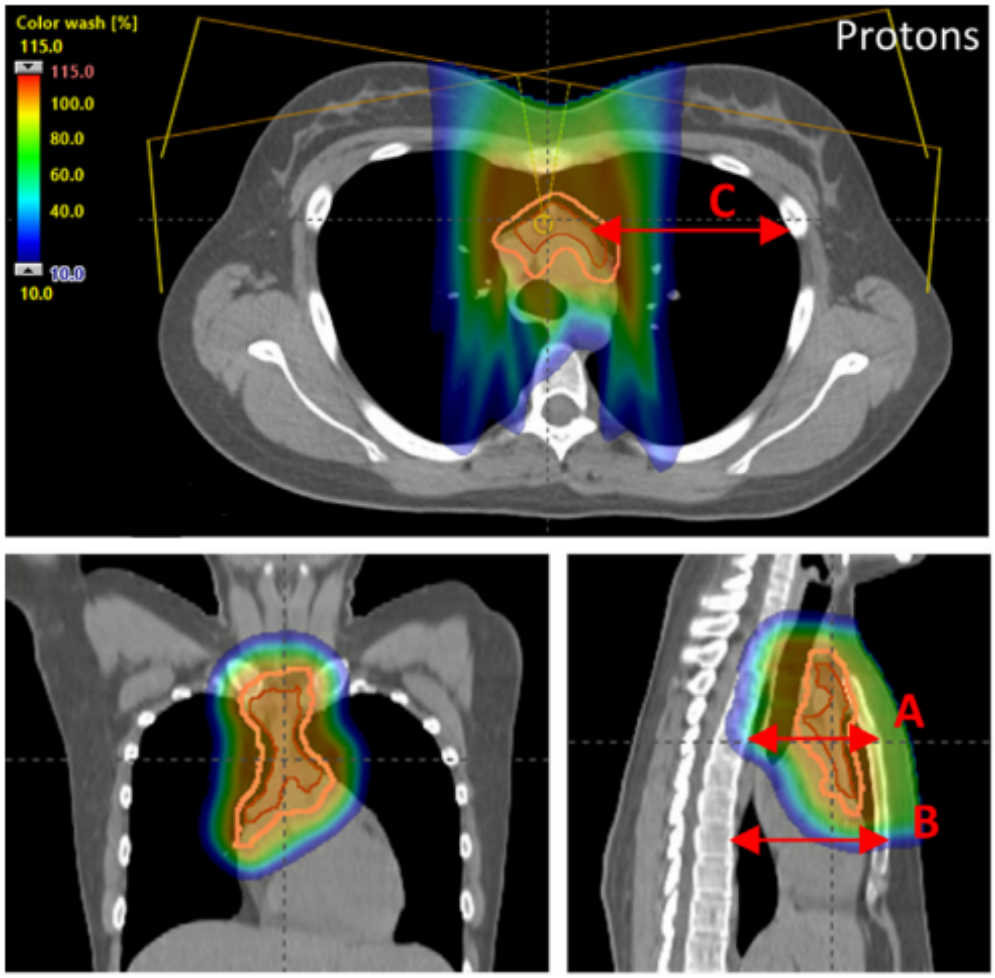

Figure 20: Examples of well-defined distances in the thorax region which can be used to assess inter breath-hold variations between CT images[12].